Internal stress distribution in DC joule-heated amorphous glass-covered microwires

2006 J. Phys.: Condens. Matter 18 2689

(http://iopscience.iop.org/0953-8984/18/9/008)

INSTITUTE OF PHYSICS PUBLISHING JOURNAL OF PHYSICS: CONDENSED MATTER

J. Phys.: Condens. Matter **18** (2006) 2689–2716 doi:10.1088/0953-8984/18/9/008

Internal stress distribution in DC joule-heated amorphous glass-covered microwires

Iordana Aştefănoaei[1], Daniel Radu[1] and Horia Chiriac[2]

[1] 'Al I Cuza' University, Faculty of Physics, Carol I Boulevard, No 11, RO-700050, Iasi, Romania
[2] National Institute of Research and Development for Technical Physics, 47 Mangeron Boulevard, Iasi 3, Romania

E-mail: iordana@uaic.ro

Received 18 July 2005, in final form 10 January 2006
Published 17 February 2006
Online at stacks.iop.org/JPhysCM/18/2689

Abstract

As known, the magnetic properties of AGCMs are determined by the radial, azimuthal and axial internal stresses induced during both the preparation process and the suitable thermal treatments of these microwires. In this paper we have proposed a theoretical model in order to determine the total internal stresses induced during the dc joule-heating thermal treatment (heating–crystallization–cooling). In this view (i) we have started from the internal stress values obtained in the preparation process, (ii) we have considered the supplementary axial tensile stresses due to the mechanical drawing of the microwire during the preparation process and (iii) we have taken into account the difference between the thermal expansion coefficients of metal and glass. We have found that (i) the maximum value of the axial stresses obtained after the thermal treatment is bigger than that obtained in the preparation process, the difference being about 450 MPa, (ii) the maximum values for the azimuthal and radial stresses decrease by $\cong$220 and $\cong$210 MPa respectively, (iii) the dimensions of the cylindrical inner core increase significantly (by $\cong$13%), which involves an increase of the degree of magnetic order in the AGCMs and consequently leads to the appearance of a large Barkhausen effect (LBE) in low axially applied magnetic fields and (iv) the reduced remanence increases from 0.90 to 0.95.

(Some figures in this article are in colour only in the electronic version)

1. Introduction

The amorphous glass-covered microwires (AGCMs) form a class of materials of great technological importance. They are receiving considerable experimental and theoretical attention, because of their superior mechanical, magnetic and electrical properties in comparison with similar counterparts.

AGCMs exhibit the giant magnetoimpedance effect, which makes them very interesting for microdevice sensors and electronic devices, also ensuring a high corrosion and mechanical resistance [1, 2]. Their magnetic, electric and structural properties strongly depend on the thermal treatment. The dc joule-heating treatment applied to AGCMs allows, for instance, the control of the internal stresses, the magnetostriction constant and the induced anisotropies. The dc joule-heating techniques are very convenient tools in studying and understanding the magnetic properties of these materials.

Usually, AGCMs are prepared by rapid quenching from the melt, using the glass-coated melt-spinning method [3]. Both the preparation method and the glass cover induce in the AGCM's metallic core large internal stresses (of about 10^9 Pa [4]). Due to these stresses, the strong magnetoelastic coupling becomes very important in the study of the magnetoelastic anisotropy. A suitable thermal treatment (for instance the dc joule-heating method) has a huge experimental—as well as theoretical—interest, because it can be used to reduce the magnetoelastic coupling. This method also allows a better control of the internal stress distribution, the magnetostriction constant and the induced anisotropy, which leads to an improvement of the AGCM's magnetic properties.

Besides, due to the internal stresses induced in the preparation process [5–7], the magnetic domain structure can be considerably modified by a proper thermal treatment. Thus, the AGCM's magnetic properties are related to the mechanical stresses induced both in the preparation and the annealing processes.

During the preparation process of the AGCMs, the induced radial, azimuthal and axial stresses have an important role in determining the magnetic properties of this type of microwires. The values and distribution of these stresses depend on the radius of the metal and on the thickness of the glass cover [4]. Unlike the conventional wires, in the case of the AGCM the internal stresses come from both the thermal process which accompanies the heating and/or cooling of the material and the constraints produced on the metal by the glass cover, as a result of the difference between the thermal expansion coefficient of the two materials.

The relatively small dimensions of the AGCMs (the diameter of the metallic part ranging between 3 and 25 μm and the thickness of the glass cover ranging between 2 and 15 μm), as well as the influence of the glass insulation on the physical properties of the metallic core, offer attractive possibilities in studying the improvement of the magnetic behaviour of these materials and open a large field of potential technological applications.

A great number of papers have been recently published on this subject. The large number of experimental data refers to the induced internal stresses and the effect of these stresses on different properties of the AGCMs [1, 2, 6]. But a systematic theoretical study on this subject, able to emphasize the spatial and temporal variation of the induced internal stresses during a thermal treatment, has not been reported yet. Therefore, the main purpose of the present paper is to determine the stresses that appear in the annealing process by a dc joule-heating treatment.

A similar study was developed by Chiriac *et al* [4], but their approach was focused on the internal stresses appearing in these structures due to the preparation process only (the glass-coated melt-spinning method).

As known [8–10], the joule-heating method usually implies the use of an electrical dc to produce (when passing through the AGCM) an electrical resistivity variation, which, in turn, leads to a variation of the developed joule power and subsequently to a corresponding variation in the temperature distribution. As will be shown in the following, this temperature variation considerably influences the internal stresses in the AGCM, leading to an improvement of their magnetic properties. It is well known that AGCMs with an $Fe_{77.5}B_{15}Si_{7.5}$ composition exhibit a positive magnetostriction, while the stresses induced in the metallic core by the radial

temperature gradients and also by the glass insulation lead to a large Barkhausen effect (LBE) in the metallic core of the samples [11, 12].

Considering at least a linear dependence of the resistivity on the temperature and the dc joule-heating effects (conduction and radiative losses, as well as the structural changes during the crystallization process), we first present a theoretical model for the determination of the radial and temporal temperature distribution, both in the metallic core and the glass cover of an AGCM. Then, the knowledge of the radial temperature distribution corresponding to a given value of the annealing electrical dc passing through the sample [13] allows the calculation of the internal stresses as a function of $I(A)$. The distribution analysis for these stresses provides useful information concerning the modifications of the annealed AGCM's magnetic properties. A comparison between our theoretical results and the experimental data will be presented at the end of this paper.

The paper is conceived as follows:

- section 1 marks an introduction;
- in section 2, we present the main aspects of the theoretical formalism which can be used in order to find the induced internal stresses both in the metallic core and in the glass cover of an AGCM subjected to a dc joule-heating annealing;
- section 3, having three subsections, presents the effective calculation of the induced stresses which appear in the three successive stages of the thermal treatment, i.e.

  (a) during the heating of the sample, until it reaches the temperature corresponding to the onset of the crystallization process,
  (b) during the crystallization process and
  (c) during the cooling of the crystallized sample until it reaches room temperature;

  for each of these stages we first determined the corresponding temperature distribution in the sample necessary to evaluate the internal stresses;
- in section 4 the total stresses are obtained starting from the internal stresses induced in the preparation process of the sample and taking into account the modifications brought by the three stages of the thermal treatment presented in the previous section;
- section 5 is dedicated to discussion and conclusions.

2. Internal stresses induced by the temperature gradient in AGCMs

In this section we calculate the internal stresses induced in AGCMs due to the joule heating of the sample during the thermal treatment, taking into account the difference between the thermal expansion coefficients of the two materials in contact (metallic core and glass cover).

In most cases, AGCMs consist in a cylindrical metallic core with a diameter of (3–25) μm, covered by glass insulation with a thickness of (2–15) μm [4].

Let us consider an AGCM, placed in vacuum at a pressure less than 10^3 Pa, subjected to a dc joule-heating thermal treatment. We assume that the cylindrical metallic core has a radius R_{m} and the glass insulation has the thickness $R_{\mathrm{w}} - R_{\mathrm{m}}$, where R_{w} is the total radius of the microwire (metal + glass). We associate a cylindrical system of coordinates (r, θ, z) with the sample, having the Oz-axis along the microwire's axis (see figure 1).

We consider that the components of the displacement vector $\vec{u}$ of any point of the microwire, namely u_r, u_θ and u_z, are independent of each other. Due to the spatial symmetry of the heating process, and implicitly of the displacements and strains generated by this process, u_θ = constant both in the metal and in the glass. Because of this we will be interested only in the radial (u_r) and axial (u_z) components of the vector $\vec{u}$.

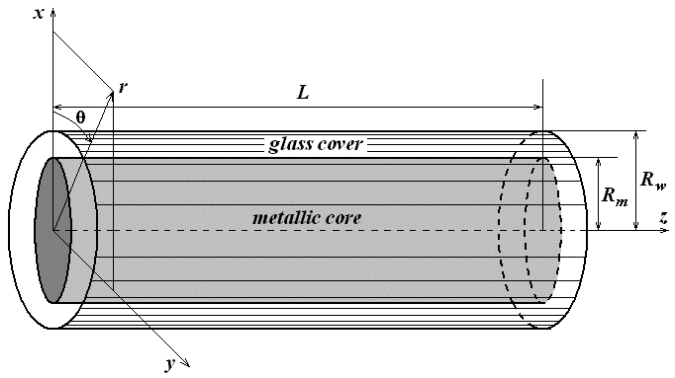

Figure 1. The spatial orientation of the AGCM. R_{m} is the radius of the metallic core and R_{w} is the total microwire's radius.

The radial temperature gradients lead to the appearance of some displacements, both in the metallic core (u_r^{m} and u_z^{m}) and in the glass insulation (u_r^{g} and u_z^{g}). These displacements satisfy the differential displacements' equation. In cylindrical coordinates this equation reads [14, 15]

$$\frac{\mathrm{d}}{\mathrm{d}r}\left[\frac{1}{r}\frac{\mathrm{d}(u_r^{\mathrm{m}}r)}{\mathrm{d}r}\right] = \frac{1+\mu}{1-\mu}\alpha_{\mathrm{m}}\frac{\mathrm{d}T(r)}{\mathrm{d}r}, \tag{1}$$

$$\frac{\mathrm{d}u_z^{\mathrm{m}}}{\mathrm{d}z} = \text{constant}, \tag{2}$$

for the metal core and

$$\frac{\mathrm{d}}{\mathrm{d}r}\left[\frac{1}{r}\frac{\mathrm{d}(u_r^{\mathrm{g}}r)}{\mathrm{d}r}\right] = \frac{1+\mu}{1-\mu}\alpha_{\mathrm{g}}\frac{\mathrm{d}t(r)}{\mathrm{d}r}, \tag{3}$$

$$\frac{\mathrm{d}u_z^{\mathrm{g}}}{\mathrm{d}z} = \text{constant}, \tag{4}$$

for the glass cover. In the above relations α_{m} and α_{g} are the metallic core's and respectively the glass cover's thermal expansion coefficients, μ is the Poisson's coefficient, $T(r)$ is the radial temperature distribution in the metallic core of the sample and $t(r)$ is the radial temperature distribution in the glass cover. It is assumed that the values of Poisson's coefficient for metal and glass are the same: $\mu_{\mathrm{metal}} = \mu_{\mathrm{glass}} = \mu = \frac{1}{3}$. The solutions of equations (1) and (2) (representing the radial, $u_r^{\mathrm{m}}(r)$ and axial, u_z^{m} displacements in the metallic core of the microwire) have the form

$$u_r^{\mathrm{m}}(r) = \frac{\alpha_{\mathrm{m}}}{r}\left(\frac{1+\mu}{1-\mu}\right)\int_0^r rT(r)\,\mathrm{d}r + \frac{C_1^{\mathrm{m}}}{2}r + \frac{C_2^{\mathrm{m}}}{r} \tag{5}$$

and respectively,

$$u_z^{\mathrm{m}} = b_{\mathrm{m}}z, \tag{6}$$

where C_1^{m}, C_2^{m} and b_{m} are the integration constants. Let us notice that in the centre of the microwire (at $r = 0$), due to the spatial symmetry of the process, there is actually no radial displacement, i.e., $u_r^{\mathrm{m}}(r=0) = 0$. This implies in relation (5) that $C_2^{\mathrm{m}} = 0$; consequently, the radial displacement $u_r^{\mathrm{m}}(r)$ becomes

$$u_r^{\mathrm{m}}(r) = \frac{\alpha_{\mathrm{m}}}{r}\left(\frac{1+\mu}{1-\mu}\right)\int_0^r rT(r)\,\mathrm{d}r + \frac{C_1^{\mathrm{m}}}{2}r. \tag{7}$$

Equations (3) and (4) have the following solutions:

$$u_r^{\mathrm{g}}(r) = \frac{\alpha_{\mathrm{g}}}{r}\left(\frac{1+\mu}{1-\mu}\right)\int_{R_{\mathrm{m}}}^{R_{\mathrm{w}}} rt(r)\,\mathrm{d}r + \frac{C_1^{\mathrm{g}}}{2}r + \frac{C_2^{\mathrm{g}}}{r} \tag{8}$$

and respectively,

$$u_z^{\mathrm{g}} = b_{\mathrm{g}}z, \tag{9}$$

where C_1^{g}, C_2^{g} and b_{g} are the integration constants. In the cylindrical coordinates, the components of the strain tensor for the metallic core (u_{rr}^{m}, $u_{\theta\theta}^{\mathrm{m}}$, u_{zz}^{m}) and for the glass cover (u_{rr}^{g}, $u_{\theta\theta}^{\mathrm{g}}$, u_{zz}^{g}) can be obtained using the displacements given by relations (6)–(9), and considering the azimuthal displacements (u_θ^{m} and u_θ^{g}) as constants. The diagonal components of the strain tensor (assuming that the other components are zero) for the metallic core are

$$u_{rr}^{\mathrm{m}} = \frac{\partial u_r^{\mathrm{m}}}{\partial r} = -\frac{\alpha_{\mathrm{m}}}{r^2}\left(\frac{1+\mu}{1-\mu}\right)\int_0^r rT(r)\,\mathrm{d}r + \frac{C_1^{\mathrm{m}}}{2} + \frac{\alpha_{\mathrm{m}}(1+\mu)T(r)}{1-\mu}, \tag{10a}$$

$$u_{\theta\theta}^{\mathrm{m}} = \frac{u_r^{\mathrm{m}}}{r} = \frac{\alpha_{\mathrm{m}}}{r^2}\left(\frac{1+\mu}{1-\mu}\right)\int_0^r rT(r)\,\mathrm{d}r + \frac{C_1^{\mathrm{m}}}{2}, \tag{10b}$$

$$u_{zz}^{\mathrm{m}} = \frac{\mathrm{d}u_z^{\mathrm{m}}}{\mathrm{d}z} = b_{\mathrm{m}} \tag{10c}$$

and for the glass cover,

$$u_{rr}^{\mathrm{g}} = \frac{\partial u_r^{\mathrm{g}}}{\partial r} = \frac{\alpha_{\mathrm{g}}(1+\mu)t(r)}{1-\mu} - \frac{\alpha_{\mathrm{g}}}{r^2}\left(\frac{1+\mu}{1-\mu}\right)\int_{R_{\mathrm{m}}}^r rt(r)\,\mathrm{d}r + \frac{C_1^{\mathrm{g}}}{2} - \frac{C_2^{\mathrm{g}}}{r^2}, \tag{11a}$$

$$u_{\theta\theta}^{\mathrm{g}} = \frac{u_r^{\mathrm{g}}}{r} = \frac{\alpha_{\mathrm{g}}}{r^2}\left(\frac{1+\mu}{1-\mu}\right)\int_{R_{\mathrm{m}}}^r rt(r)\,\mathrm{d}r + \frac{C_1^{\mathrm{g}}}{2} + \frac{C_2^{\mathrm{g}}}{r^2}, \tag{11b}$$

$$u_{zz}^{\mathrm{g}} = \frac{\mathrm{d}u_z^{\mathrm{g}}}{\mathrm{d}z} = b_{\mathrm{g}}. \tag{11c}$$

As follows from figure 1 for the metallic core, the range in which the radial coordinate r takes values in the metallic region is $(0,\ R_{\mathrm{m}}]$, whereas for the glass cover the same coordinate takes values in the interval $(R_{\mathrm{m}},\ R_{\mathrm{w}}]$.

The diagonal components of the stress tensor in the metallic core (σ_{rr}^{m}, $\sigma_{\theta\theta}^{\mathrm{m}}$, σ_{zz}^{m}), as well as in the glass cover (σ_{rr}^{g}, $\sigma_{\theta\theta}^{\mathrm{g}}$, σ_{zz}^{g}), can be determined using the generalized Hooke's law:

$$\sigma_{ik} = \frac{E}{1+\mu}\left[u_{ik} + \frac{\mu}{1-2\mu}u_{ll}\delta_{ik}\right]. \tag{12}$$

Thus, substituting the strain tensor components given by relations (10) in the Hooke's law (12) for the diagonal components of the stress tensor in the metallic core, we give the following expressions:

$$\sigma_{rr}^{\mathrm{m}} = \frac{E_{\mathrm{m}}(C_1^{\mathrm{m}} + 2\mu b_{\mathrm{m}})}{2(1+\mu)(1-2\mu)} - \frac{E_{\mathrm{m}}\alpha_{\mathrm{m}}}{r^2(1-\mu)}\int_0^r rT(r)\,\mathrm{d}r, \tag{13a}$$

$$\sigma_{\theta\theta}^{\mathrm{m}} = \frac{E_{\mathrm{m}}(C_1^{\mathrm{m}} + 2\mu b_{\mathrm{m}})}{2(1+\mu)(1-2\mu)} + \frac{E_{\mathrm{m}}\alpha_{\mathrm{m}}}{r^2(1-\mu)}\int_0^r rT(r)\,\mathrm{d}r - \frac{\alpha_{\mathrm{m}}E_{\mathrm{m}}T(r)}{1-\mu} \tag{13b}$$

and

$$\sigma_{zz}^{\mathrm{m}} = \frac{E_{\mathrm{m}}(C_1^{\mathrm{m}} + 2\mu b_{\mathrm{m}})}{(1+\mu)(1-2\mu)} - \frac{\alpha_{\mathrm{m}}E_{\mathrm{m}}T(r)}{1-\mu}. \tag{13c}$$

Accordingly, using the relations (11) and (12) for the diagonal components of the stress tensor in the glass cover we obtain the following expressions:

$$\sigma_{rr}^{\mathrm{g}} = \frac{E_{\mathrm{g}}(C_1^{\mathrm{g}} + 2\mu b_{\mathrm{g}})}{2(1+\mu)(1-2\mu)} - \frac{E_{\mathrm{g}}\alpha_{\mathrm{g}}}{r^2(1-\mu)}\int_{R_{\mathrm{m}}}^{r} rt(r)\,\mathrm{d}r - \frac{E_{\mathrm{g}}C_2^{\mathrm{g}}}{(1+\mu)r^2}, \tag{14a}$$

$$\sigma_{\theta\theta}^{\mathrm{g}} = \frac{E_{\mathrm{g}}(C_1^{\mathrm{g}} + 2\mu b_{\mathrm{g}})}{2(1+\mu)(1-2\mu)} + \frac{E_{\mathrm{g}}\alpha_{\mathrm{g}}}{r^2(1+\mu)}\int_{R_{\mathrm{m}}}^{r} rt(r)\,\mathrm{d}r + \frac{E_{\mathrm{g}}C_2^{\mathrm{g}}}{(1+\mu)r^2} - \frac{\alpha_{\mathrm{g}}E_{\mathrm{g}}t(r)}{1-\mu} \tag{14b}$$

and

$$\sigma_{zz}^{\mathrm{g}} = \frac{E_{\mathrm{g}}(C_1^{\mathrm{g}} + 2\mu b_{\mathrm{g}})}{(1+\mu)(1-2\mu)} - \frac{\alpha_{\mathrm{g}}E_{\mathrm{g}}t(r)}{1-\mu}. \tag{14c}$$

In relations (13) and (14) E_{m} and E_{g} are the Young's moduli for the metal and for the glass, respectively.

We will now determine the resultant strain due to the different heating of the two materials with different thermal expansion coefficients, being in contact during the entire thermal process. As is well known, the law of the linear thermal expansion is

$$l = l_0(1 + \alpha\Delta T) \tag{15}$$

in which l is the linear dimension of the sample in the chosen direction, at the temperature T, l_0 is the same linear dimension at the temperature T_0, $\Delta T = T(r = R_{\mathrm{m}}) - T_0$ is the temperature range in which the variation $\Delta l = l - l_0$ takes place, and α is the thermal expansion coefficient. From (17) we have for the metal region

$$\varepsilon_{\mathrm{m}} = \alpha_{\mathrm{m}}(T(r = R_{\mathrm{m}}) - T_0), \tag{16}$$

and for the glass cover

$$\varepsilon_{\mathrm{g}} = \alpha_{\mathrm{g}}(t(r = R_{\mathrm{m}}) - T_0), \tag{17}$$

where ε_{m} and ε_{g} are the strains due to the thermal contraction in the metal and glass respectively, and α_{m} and α_{g} are the corresponding thermal expansion coefficients. Because of the continuity of the temperature fields at the point $r = R_{\mathrm{m}}$, $T(r = R_{\mathrm{m}}) = t(r = R_{\mathrm{m}})$, it follows that the resultant strain is

$$\varepsilon = \varepsilon_{\mathrm{m}} - \varepsilon_{\mathrm{g}} = (\alpha_{\mathrm{m}} - \alpha_{\mathrm{g}})\Delta T. \tag{18}$$

In our case, ΔT is the difference between room temperature and the temperature at the point $r = R_{\mathrm{m}}$. During the thermal treatment of the microwire, due to the difference between the thermal expansion coefficients of glass and metal, the glass cover induces specific tensions in the metallic core. In order to find the resultant stress tensor components, σ_{rr}^{m}, $\sigma_{\theta\theta}^{\mathrm{m}}$, σ_{zz}^{m}, σ_{rr}^{g}, $\sigma_{\theta\theta}^{\mathrm{g}}$ and σ_{zz}^{g}, we must calculate the values of the constants C_1^{m}, C_1^{g}, C_2^{g}, b_{m} and b_{g}, taking into account the different values of the thermal expansion coefficients of the two materials (metal and glass). This can be done using the equilibrium conditions that must be satisfied by the stresses which appear both at the metal–glass interface,

$$\sigma_{rr}^{\mathrm{m}}(r = R_{\mathrm{m}}) - \sigma_{rr}^{\mathrm{g}}(r = R_{\mathrm{m}}) = 0, \tag{19}$$

$$\sigma_{zz}^{\mathrm{m}}(r = R_{\mathrm{m}}) + S\sigma_{zz}^{\mathrm{g}}(r = R_{\mathrm{m}}) = 0 \tag{20}$$

and at the exterior surface of the microwire,

$$\sigma_{rr}^{\mathrm{g}}(r = R_{\mathrm{w}}) = 0. \tag{21}$$

First of all, the following conditions have to be imposed, so that all the strains appearing in this process are due only to the difference between the thermal expansion coefficients of the metal and glass:

$$u_z^{\mathrm{m}}(r = R_{\mathrm{m}}) - u_z^{\mathrm{g}}(r = R_{\mathrm{m}}) = \varepsilon z \tag{22}$$

and

$$u_r^{\mathrm{m}}(r = R_{\mathrm{m}}) - u_r^{\mathrm{g}}(r = R_{\mathrm{m}}) = \varepsilon R_{\mathrm{m}}. \tag{23}$$

In relation (20), $S = \frac{S_{tr}^{\mathrm{g}}}{S_{tr}^{\mathrm{m}}} = \frac{R_{\mathrm{w}}^2}{R_{\mathrm{m}}^2} - 1$, where S_{tr}^{g} and S_{tr}^{m} are the cross section areas of the glass cover and of the metallic core, respectively. Therefore, substituting the expressions for σ_{rr}^{m}, σ_{zz}^{m}, σ_{rr}^{g}, σ_{zz}^{g}, u_r^{m}, u_z^{m}, u_r^{g} and u_z^{g} in relations (22), (23) and (19)–(21) we get the following five-equation algebraic system:

$$b_{\mathrm{m}} - b_{\mathrm{g}} = \varepsilon, \tag{24}$$

$$\frac{1}{R_{\mathrm{m}}^2}\left(\frac{1+\mu}{1-\mu}\right)\int_0^{R_{\mathrm{m}}} r(\alpha_{\mathrm{m}} T(r) - \alpha_{\mathrm{g}} t(r))\,\mathrm{d}r + (C_1^{\mathrm{m}} - C_1^{\mathrm{g}}) - \frac{C_2^{\mathrm{g}}}{R_{\mathrm{m}}^2} = \varepsilon, \tag{25}$$

$$\frac{E_{\mathrm{m}}(C_1^{\mathrm{m}} + \mu b_{\mathrm{m}})}{(1+\mu)(1-2\mu)} - \frac{E_{\mathrm{m}}\alpha_{\mathrm{m}}}{(1-\mu)R_{\mathrm{m}}^2}\int_0^{R_{\mathrm{m}}} rT(r)\,\mathrm{d}r = \frac{E_{\mathrm{g}}(C_1^{\mathrm{g}} + \mu b_{\mathrm{g}})}{(1+\mu)(1-2\mu)} - \frac{E_{\mathrm{g}}C_2^{\mathrm{g}}}{(1+\mu)R_{\mathrm{m}}^2}, \tag{26}$$

$$\frac{2\mu E_{\mathrm{m}}(C_1^{\mathrm{m}} + \mu b_{\mathrm{m}})}{(1+\mu)(1-2\mu)} - \frac{\alpha_{\mathrm{m}} E_{\mathrm{m}} T(r = R_{\mathrm{m}})}{1-\mu} + \frac{2\mu S E_{\mathrm{g}}(C_1^{\mathrm{g}} + \mu b_{\mathrm{g}})}{(1+\mu)(1-2\mu)} - \frac{\alpha_{\mathrm{g}} S E_{\mathrm{g}} t(r = R_{\mathrm{m}})}{1-\mu} = 0, \tag{27}$$

$$\frac{C_1^{\mathrm{g}} + \mu b_{\mathrm{g}}}{(1+\mu)(1-2\mu)} - \frac{C_2^{\mathrm{g}}}{(1+\mu)R_{\mathrm{w}}^2} = \frac{\alpha_{\mathrm{g}}}{(1-\mu)R_{\mathrm{w}}^2}\int_{R_{\mathrm{m}}}^{R_{\mathrm{w}}} rt(r)\,\mathrm{d}r, \tag{28}$$

with the five unknowns C_1^{m}, C_1^{g}, C_2^{g}, b_{m} and b_{g}. These constants result as a solution of this system. Using this solution in relations (13) and (14) we finally get the expressions of the internal stresses induced by the radial temperature gradient, taking into account the difference between the two thermal expansion coefficients (of metal and glass) during the thermal treatment by dc joule heating of AGCMs.

Therefore, the internal stresses induced by the thermal gradients both in the metallic core (σ_{rr}^{m}, $\sigma_{\theta\theta}^{\mathrm{m}}$, σ_{zz}^{m}) and in the glass cover (σ_{rr}^{g}, $\sigma_{\theta\theta}^{\mathrm{g}}$ and σ_{zz}^{g}) during a thermal treatment of the AGCM are given by relations (13) and (14) together with the five constants C_1^{m}, C_1^{g}, C_2^{g}, b_{m} and b_{g} (obtained as the solution of the equation system (24)–(28)).

3. Internal stresses induced during the dc joule-heating treatment

The so-called technique of dc joule heating involves relatively low electrical currents (up to 4 A) which pass through the sample for long times (1–100) s and emerges as the natural choice when the details of the structural transformations occurring within the sample have to be known with accuracy [9].

In this section we analyse the thermal behaviour of AGCMs and the internal stress distribution during dc joule heating, taking into account the linear dependence of the electrical resistivity on temperature and the structural changes during the crystallization process. The theoretical and experimental considerations refer separately to the two different situations, namely

(1) the amorphous state, when the temperature values are below the onset temperature of crystallization, and

(2) the transition from the amorphous to the crystalline state, when both phases appear.

In order to calculate the internal stresses distribution we will analyse the temporal and radial distribution of the temperature in the transient and steady states, taking into account the dc joule-heating effects (conduction and radiative heat losses) [16].

3.1. Internal stresses induced in AGCMs below the onset of the crystallization process

In this subsection we analyse a theoretical model for the stress distribution induced by the thermal dilatation of the amorphous glass-covered microwires, during dc joule heating, below the onset of the crystallization process (in the amorphous phase of the sample).

So, let us consider an AGCM in the same conditions as above (i.e. placed in vacuum at a pressure less than 10^3 Pa), through which a dc current passes. We will calculate the temporal and radial temperature distributions in the transient and steady states, taking into account the linear dependence of the electrical resistivity on temperature. We assume that the heat loss by the Thomson effect is negligible (the ends of the sample are thermally isolated) and we will not explicitly consider the structural changes appearing in the electrical resistivity below crystallization temperature.

In our theoretical model we neglect the resistivity variations due to structural processes during annealing below the crystallization temperature. A few per cent variation of resistivity can be experimentally observed in the case when the annealing temperature is approaching the crystallization temperature but has to be verified on a per case basis. This fact has no significant consequences because, as follows from the electrical resistivity measurements [17, 18], these changes represent only a small percentage of the resistivity variation with temperature. The effect of the structural changes on the electrical resistivity becomes significant only for those values of the dc leading to temperatures close to the crystallization one. In order to determine the temperature distribution in an AGCM annealed by the joule effect, we use the Fourier heat conduction equation with the boundary conditions required by the existence of the metal–glass interface and by the surface heat losses.

3.1.1. Temperature distribution in dc joule-heated AGCMs

(a) Temperature distribution in the metallic core. As we can see from (13) and1 (14), the calculation of the internal stresses demands the knowledge of the radial temperature distributions, $T = T(r)$ (in the metallic core) and $t = t(r)$ (for the glass insulation). Thus, our following purpose is to determine these two temperature fields.

In the transient state the energy developed by the joule effect is consumed to increase the sample's internal energy, whereas in the steady state the joule energy ensures the heating of the glass insulation of the AGCM in order to compensate the thermal losses through the microwire surface.

The heat developed in unit volume by the joule effect in the metallic core has the form

$$W_i = \rho_{\mathrm{m}} j^2(r) = \rho_0 \{1 + \alpha [T_{\mathrm{m}}(r, t) - T_0]\} j^2(r), \tag{29}$$

where $\rho_{\mathrm{m}} = \rho_{\mathrm{m}}(r,\ t)$ is the resistivity at temperature $T_{\mathrm{m}}(r,\ t)$, α is the thermal coefficient of the resistivity, t is the time during which the electrical current passes through the sample, ρ_0 is the resistivity at the room temperature (T_0), and $j(r)$ is the current density distribution in the sample. We assume that [16]

$$j(r) \equiv j = \frac{I}{S} = \text{constant}.$$

The heat generated in the sample is a function of r and t (time), for each value of the electrical current, $I(A)$. In the transient state the energy conservation law for the sample becomes

$$\rho_{\mathrm{M}} c \frac{\mathrm{d}T}{\mathrm{d}t} = (\rho_\infty - \rho_{\mathrm{m}}) \frac{I^2}{S^2}, \tag{30}$$

where ρ_{M} is the mass density, c is the specific heat and $\rho_\infty = \rho_\infty(r)$ is the electrical resistivity in the steady state. The temperature field $T_{\mathrm{m}}(r,\ t)$ can be obtained by integrating (30), taking into account (29). The result is

$$T_{\mathrm{m}}(r,t) = T_0 + [T_{\mathrm{m}}(r) - T_0]\left[1 - \exp\left(-\frac{\alpha\rho_0 I^2}{c\rho_{\mathrm{M}} S_1^2} t\right)\right]. \tag{31}$$

Here $T_{\mathrm{m}}(r)$ is the temperature of the microwire's metallic core in the steady state (at the thermal equilibrium) and $S_1 = \pi R_{\mathrm{m}}^2$ is the cross-section of the metallic core. Using the Fourier heat conduction equation [19]

$$\frac{1}{r}\frac{\mathrm{d}}{\mathrm{d}r}\left(\frac{\mathrm{d}T_{\mathrm{m}}(r)}{\mathrm{d}r}\right) + \frac{W_i}{k_{\mathrm{m}}} = 0 \tag{32}$$

and the expressions corresponding to the initial conditions

$$T_{\mathrm{m}}(r,\ I=0) = T_0, \qquad \rho_{\mathrm{m}}\,(r,\ I=0) = \rho_0, \tag{33}$$

we obtained the radial temperature distribution $T_{\mathrm{m}}(r)$ in the metallic core of the AGCM, at thermal equilibrium (in steady state, $t \to \infty$):

$$T_{\mathrm{m}}(r) = T_0 - \alpha^{-1} + C(I) J_0\left(r\sqrt{\alpha\rho_0 I^2 k_{\mathrm{m}}^{-1} S_1^{-2}}\right), \tag{34}$$

where J_0 are the zero-order Bessel functions, k_{m} is the thermal conductivity of the metallic core and $C = C(I)$ is the integration 'constant', that is a function of the electrical current $I(A)$. For $I = 0$, from (33) and (34), it follows that $C(0) = \alpha^{-1}$. The electrical resistivity in the steady state, $\rho_\infty(r)$, is given by the relation

$$\rho_\infty(r) = \rho_0 C(I)\alpha J_0\left(r\sqrt{\alpha\rho_0 I^2 k^{-1} S^{-2}}\right). \tag{35}$$

In order to determine the temperature distribution in the metallic core, the corresponding boundary conditions must be considered.

(b) Temperature distribution in the glass insulation. In the steady state ($t \to \infty$), the thermal equilibrium between the sample and the environmental medium is achieved. In this case, the heat flux from the metallic core—generated by the joule effect—is received by the glass insulation. Using the Fourier heat conduction equation for $R_{\mathrm{m}} < r < R_{\mathrm{w}}$,

$$\frac{1}{r}\frac{\mathrm{d}}{\mathrm{d}r}\left(r\frac{\mathrm{d}T_{\mathrm{g}}(r)}{\mathrm{d}r}\right) = 0, \tag{36}$$

we now calculate the equilibrium temperature of the glass insulation, $T_{\mathrm{g}}(r)$. The general solution of equation (36) reads

$$T_{\mathrm{g}}(r) = A_1 \ln r + A_2, \tag{37}$$

where the integration 'constants' $A_1 = A_1(I)$ and $A_2 = A_2(I)$ are functions of the same parameter $I(A)$, their physical significance appearing in the following subsection.

(c) Boundary conditions for the metal–glass interface. In order to determine the final expressions for the temperature $T_m(r)$ in the metallic core (34) and in the glass insulation (37), we must use the following boundary conditions:

(i) in the thermal steady state, the heat flux from the metallic core is received by the glass insulation. This heat flux (from the metal–glass interface) must be continuous. So, for $r = R_m$ we must have

$$k_m(dT_m/dr) = k_g(dT_g/dr), \tag{38}$$

where k_m and k_g are the coefficients of thermal conductivity for the amorphous metallic core and glass insulation, respectively;

(ii) on the metal–glass interface ($r = R_m$), the temperatures from the adjacent regions must be equal:

$$T_m(R_m) = T_g(R_m); \tag{39}$$

(iii) in the steady state ($t \to \infty$), on the outer surface of the microwire, the thermal equilibrium between the sample and the environmental medium is achieved by radiative heat loss:

$$-\left.\frac{dT_g}{dr}\right|_{r=R_w} = Pk_g^{-1}[T^4(R_w) - T_0^4], \tag{40}$$

where $P = 2\sigma eL/R_w$ is the so-called *microwire's loss parameter*, while L is the length of the sample.

Using the boundary conditions given by (38), (39) and (40) we get the following relations:

$$-k_m k_g^{-1} R_m C(I)\sqrt{\alpha\rho_0 I^2(k_m\pi^2 R_m^4)^{-1}}\, J_1\left(R_m\sqrt{\alpha\rho_0 I^2(k_m\pi^2 R_m^4)^{-1}}\right) = A_1, \tag{41}$$

$$A_1 \ln R_m + A_2 = T_0 - \alpha^{-1} + C(I) J_0\left(R_m\sqrt{\alpha\rho_0 I^2(k_m\pi^2 R_m^4)^{-1}}\right) \tag{42}$$

and

$$A_1 \ln R_w + A_2 = \left[T_0^4 - A_1 k_m (R_w P)^{-1}\right]^{1/4}, \tag{43}$$

where J_1 are the first-order Bessel functions. From (41), (42) and (43) we obtain $C(I)$, $A_1 = A_1(I)$ and $A_2 = A_2(I)$ as follows.

The 'constant' $A_1 = A_1(I)$ results as a numerical solution of the following transcendent equation:

$$A_1\left[\ln\left(\frac{R_m}{R_w}\right) + \frac{k_g S_1}{R_m I\sqrt{k_m\alpha\rho_0}}\frac{J_0\left(R_m\sqrt{\alpha\rho_0 I^2(k_m\pi^2 R_m^4)^{-1}}\right)}{J_1\left(R_m\sqrt{\alpha\rho_0 I^2(k_m\pi^2 R_m^4)^{-1}}\right)}\right] = T_0 - \frac{1}{\alpha} - \left(T_0^4 - \frac{A_1}{PR_w}\right)^{1/4}. \tag{44}$$

For each given value of the annealing current $I(A)$, one can obtain a corresponding numerical value of the 'constant' $A_1 = A_1(I)$. Then, the numerical values of $C(I)$ simply result from

$$C(I) = -k_g S_1\left(R_m I\sqrt{k_m\alpha\rho_0}\right)^{-1} A_1\left[J_1\left(R_m\sqrt{\alpha\rho_0 I^2(k_m\pi^2 R_m^4)^{-1}}\right)\right]^{-1}, \tag{45}$$

where A_1 (already known) must be introduced. At the same time, the constant A_2 results immediately from (43). We observe that the parameter $C(I)$ depends on the electrical current $I = I(A)$, the material constants α, ρ_0, k_m, k_g and the sample's dimensions: R_m, R_g and

Table 1. The characteristics of the amorphous sample.

Characteristic quantity	Significance	Value and measurement units
c	Specific heat	530 J kg^{-1} K^{-1}
e	Coefficient of the thermal emittance	0.43
k_{m}	Thermal conductibility of the metallic core	30 W mK^{-1}
k_{g}	Thermal conductibility of the glass insulation	1.177 W mK^{-1}
ρ_{M}	Mass density	7.2×10^3 kg m^{-3}
ρ	Resistivity at the room temperature	1.24×10^{-6} Ω m
T_0	Room temperature	293 K
L	Length of the sample	250 mm
R_{m}	Radius of the metallic core	9 μm
R_{w}	Radius of the amorphous glass-covered microwire	18 μm

Table 2. The numerical values of $C(I)$, $A_1(I)$ and $A_2(I)$ for different values of the electrical dc, $I(A)$.

No.	I (mA)	$C(I)$	$A_1 = A_1(I)$	$A_2 = A_2(I)$
1	1	5772.63	−0.001	58.3385
2	5	5845.17	−0.018	130.681
3	7	5869.32	−0.035	154.632
4	9	5890.25	−0.058	175.293
5	14	5934.20	−0.140	218.287
6	17.8	5962.61	−0.229	245.668
7	21	5984.30	−0.320	266.308
8	23	5997.06	−0.383	278.309
9	25	6009.28	−0.454	289.715
10	27	6021.05	−0.530	300.588
11	28	6026.78	−0.571	305.841

L. For different values of the electrical current $I(A)$, the structural changes (metastable phase relaxations) take place in the metallic region of the microwire. Consequently, the $C(I)$ parameter is called *the coefficient of metastable phase relaxations* and it explicitly contains the influences of the structural transformations that occur in the material due to the heat treatment itself.

For the amorphous glass-covered microwire's characteristics given in table 1 we have found the numerical values for $C(I)$, $A_1(I)$ and $A_2(I)$ as numerical solutions of nonlinear equations (43), (44) and (45), for 11 given values of the electrical dc in the interval $I \in$ [1–28] mA (table 2). The higher the value of the direct current $I(A)$, the higher $C(I)$, $A_1(I)$ and $A_2(I)$ are.

By introducing the numerical values of $C(I)$, $A_1(I)$ and $A_2(I)$ in the general relations (31), (34) and (37) we have obtained

(i) the spatial temperature distribution, $T_{\mathrm{m}}(r)$, in the steady state (at the thermal equilibrium) in the microwire's metallic core:

$$T_{\mathrm{m}}(r) = T_0 - \alpha^{-1} + C(I) J_0 \left(r \sqrt{\alpha \rho_0 I^2 k_{\mathrm{m}}^{-1} S_1^{-2}} \right); \tag{46}$$

(ii) the spatio-temporal temperature distribution, $T_{\mathrm{m}}(r, t)$, in the joule-heated AGCMs, in the temperature region situated below the one corresponding to the onset of the crystallization

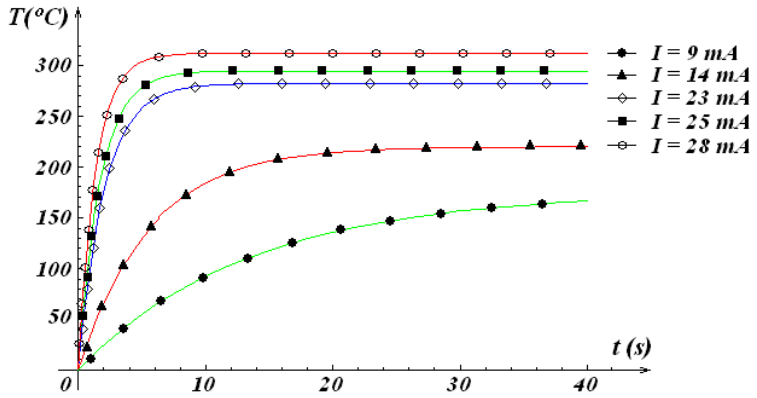

Figure 2. The temporal evolution of temperature $T(t)$ in the centre of the AGCM.

process:

$$T_{\mathrm{m}}(r,t) = T_0 + \left[C(I)J_0\left(rIS_1^{-1}\sqrt{\alpha\rho_0 k_{\mathrm{m}}^{-1}}\right) - \alpha^{-1}\right]\left[1 - \exp\left(-\frac{\alpha\rho_0 I^2}{c\rho_{\mathrm{M}}S_1^2}t\right)\right]; \tag{47}$$

(iii) the temperature distribution, $T_{\mathrm{g}}(r)$, in the steady state (at the thermal equilibrium) in the microwire's glass insulation:

$$T_{\mathrm{g}}(r) = A_1(I)\ln r + A_2(I), \tag{48}$$

the transient temperature in the microwire's glass insulation being not relevant.

On the basis of the established relations (46), (47) and (48) with the numerical values of $C(I)$, $A_1(I)$ and $A_2(I)$ we have calculated the temporal evolution and radial distribution of temperature at different values of the direct current which passes through an AGCM with a $Fe_{77.5}Si_{7.5}B_{15}$ composition and the above mentioned characteristics. With the aid of relations (29), (31) and (34), we can also obtain the electrical resistivity of the AGCM's metallic core in the transient state:

$$\rho_{\mathrm{m}}(r,t) = \rho_0 + \rho_0\left[C(I)\alpha J_0\left(r\sqrt{\alpha\rho_0 I^2 k^{-1}S_1^{-2}}\right) - 1\right]\left[1 - \exp\left(-\alpha\rho_0 I^2\rho_{\mathrm{M}}^{-1}c^{-1}S_1^{-2}t\right)\right]. \tag{49}$$

Figure 2 presents the temporal evolution of the temperature for different values of the dc $I(A)$. In this figure we observe an increase of temperature with time during which the electrical current passes through the sample, until it reaches the maximum equilibrium value. The higher the value of the direct current, the faster the maximum value of the temperature is reached.

Figure 3 illustrates the temperature distribution at the thermal equilibrium in the AGCM's cross-section for a dc value of $I = 17.8$ mA. As this figure shows, the temperature difference between the centre of the microwire's metallic core and its glass insulation is very small ($\widetilde{=}0.004\,^{\circ}$C), and that between its centre and its outer glass surface is of $\widetilde{=}0.0163\,^{\circ}$C. Thus, we can consider that the temperature is practically constant in the metallic core's cross section, and so the joule effect annealing ensures a uniform heating of the sample. We also observe an important decrease of the equilibrium temperature $T_{\mathrm{g}}(r)$ in the microwire's glass insulation ($R_{\mathrm{m}} < r < R_{\mathrm{w}}$) due to the radiative heat losses.

Using the proposed theoretical model we can calculate the maximum values reached by the temperature in the samples for different values of the applied dc.

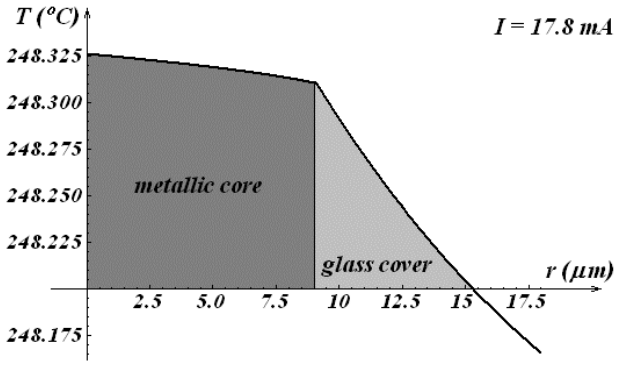

Figure 3. The temperature distribution at the thermal equilibrium in the microwire's cross-section for an electrical dc value of $I = 17.8$ mA.

3.1.2. Internal stresses induced by the radial temperature gradients. In this subsection, we will calculate, using the temperature distribution (47), the internal stress distribution induced in an AGCM through which an electrical dc of $I(A)$ intensity passes. Applying to AGCM (with characteristics presented in table 1) an electrical dc of $I = 7$ mA (with the aid of (47) and (48) in the system (24)–(28)) we calculate the five constants, C_1^{m}, C_1^{g}, C_2^{g}, b_{m} and b_{g}, that will be used in relations (13). We so determine the internal stress distribution induced by the glass cover in the metallic core of AGCM, due to the different dilatation effects of the two materials in contact. For the same value of the electrical dc ($I = 7$ mA), figure 4 shows the radial distribution of the internal stresses induced during the heating of the sample until the onset of the crystallization process, in the metallic core.

As we see from figure 4, the internal stresses σ_{rr}^{m}, $\sigma_{\theta\theta}^{\mathrm{m}}$ and σ_{zz}^{m} present a continuous increasing of their values until they reach the maximum values at the metal–glass interface, which are about 10^8 Pa. A quick comparison between the values of stresses achieved after the preparation process [4] and those obtained at the end of the first stage of the treatment emphasizes a decrease of these stresses, by approximately one order of magnitude. Also, as a consequence of the negligible variation of the radial temperature in the section of the microwire, comes a very small global relative variation of the stresses' values, of about $\widetilde{=}0.0016\%$. Another important feature of this stage of the treatment is that referring to the variation of the stresses as a function of the samples' dimensions. Thus, one can find that

- for the same radius of the metallic core, the higher the thickness of the glass cover, the higher the stresses' values are, and
- for the same value of the glass cover's thickness, the higher the radius of the metallic core, the smaller the stresses' values are.

Now, let us focus our attention on the variation of the internal stresses induced in the AGCM with $R_{\mathrm{m}} = 3.65$ μm and $R_{\mathrm{w}} = 11.15$ μm after $t = 20$ s at the beginning of the joule-heating process, for different values of the applied electrical dc, $I(A)$. The results of this analysis are given in table 3, which contains the maximum values of the internal stresses induced in the metallic core during the dc joule heating for the microwire having the characteristics given in table 1. At a first glance we see that the higher the electrical dc value, the smaller the internal stresses are. This behaviour is in good agreement with the results presented in the literature [20].

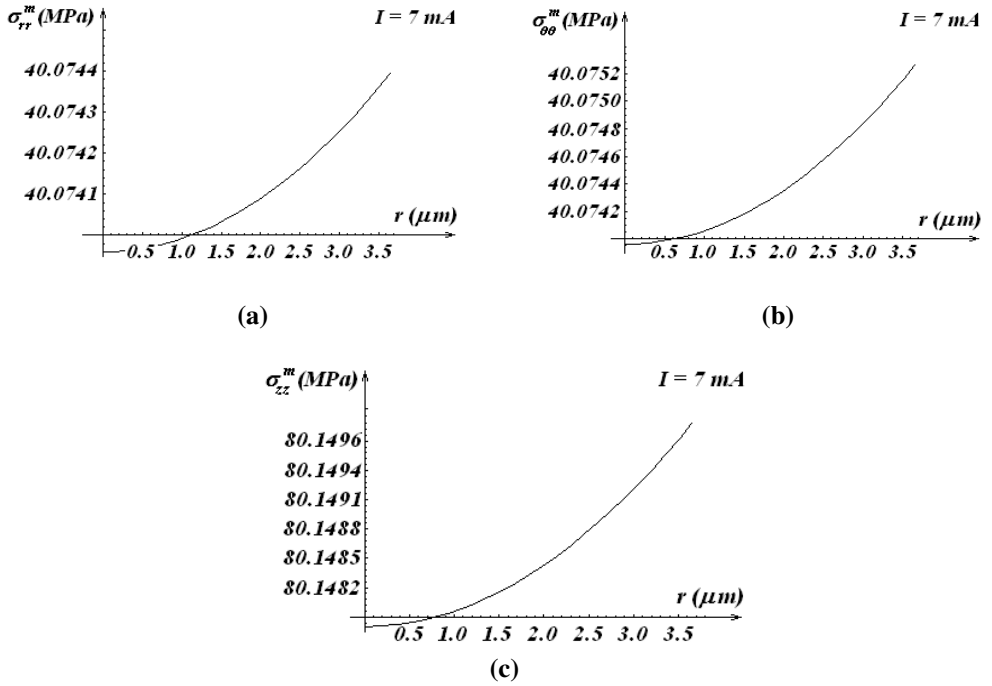

Figure 4. Internal radial, azimuthal and axial stresses' distributions for a given electrical dc value of $I = 7$ mA.

Table 3. The maximum values of the internal stresses for different values of the electrical dc.

No.	I (mA)	$\sigma_{rr}^{\max}$ (MPa)	$\sigma_{\theta\theta}^{\max}$ (MPa)	$\sigma_{zz}^{\max}$ (MPa)
1	1	96.2	96.2	192
2	5	40.3	40.3	80.6
3	7	40.07	40.07	80.14
4	9	40.05	40.06	80.3
5	14	39.8	39.8	79.6
6	23	38.6	38.6	77.23

3.2. Internal stresses induced during the crystallization process

In this section we will analyse the internal stress distribution induced during the non-isothermal crystallization processes in joule-heated AGCMs. We first present a theoretical (and the associated numerical) model able to describe the kinetics of the non-isothermal crystallization mechanism. Then, using the obtained results, we evaluate the internal stresses induced in the AGCM structure during the crystallization process.

3.2.1. Thermal behaviour and crystallization kinetics analysis of the AGCMs. In this subsection, we develop a numerical model within the context of the classical theory of phase evolution applied to AGCMs to simulate the kinetics of nucleation during the non-isothermal crystallization process. The aim of this study is to analyse the thermal behaviour and internal stress distribution of the joule-heated amorphous glass-covered microwires in such conditions. More precisely, we present a numerical model for the time evolution of the

sample's temperature and for the volume fraction crystallized with time, $x(t)$, assuming that the crystal growth and the Avrami crystallization rate constant have an Arrhenius type temperature dependence, $K = K(T)$. We also consider that the nucleation frequency K_0 is constant.

There are several methods to describe the crystallization kinetics. The most common approach used in this regard is the Johnson–Mehl–Avrami (JMA) model [19], in which the relative crystallinity is a function of time, $x = x(t)$. From the direct experimental observations, it is known that the crystallization process in the joule heated AGCMs is an exothermal one. The energy developed by the joule effect is consumed in the crystallization process to increase the internal energy of the sample and to compensate the radiative heat losses. The increase of the applied dc $I(A)$ gives rise to an increase of the electrical resistivity, and subsequently leads to a corresponding increase of internal energy. The final temperature of the sample results from the balance between the applied electrical power and the dissipation effects in the fully crystallized sample. For a more accurate picture of the process, we consider in our model the following hypotheses:

- the structure dependent parameters like ρ_{M} (the mass density of the metallic core) and c (specific heat) are constant;
- the thermal emittance coefficient, e, is also constant during the heating treatment;
- the results obtained in the above section showed that, for different values of the applied dc, the temperature of the sample is approximately constant in the whole cross-section of the metallic core. For this reason we will neglect in the following the conduction heat losses and assume that the temperature in the metallic core's cross-section is constant.

In our model, the energy released during the crystallization process appears to be a function of temperature rather than time, as in the case of the isothermal crystallization, because the non-isothermal crystallization process may be considered as composed of a great number of infinitesimally small isothermal crystallization steps. The crystallization rate parameter can be described by the exponential relation (Arrhenius form) as follows:

$$K(T) = K_0 \exp\left(-nQ/kT\right), \tag{50}$$

where Q is the growth or diffusion activation energy, T is the absolute temperature and k is the Boltzmann constant. The activation energy Q is strongly dependent on the type of nucleation in the crystallization process. The rate of transformation in the non-isothermal crystallization process is given by the relation [21]

$$\frac{\mathrm{d}x(t)}{\mathrm{d}t} = n\left[1 - x(t)\right]\left\{-\ln\left[1 - x(t)\right]\right\}^{\frac{n-1}{n}} K_0^{(1/n)} \exp\left(-\frac{Q}{kT}\right). \tag{51}$$

In order to analyse the thermal behaviour and the crystallization processes of the AGCMs we introduce a new timescale, whose zero coincides with the onset of the crystallization process, at the steady-state temperature value of the heated amorphous sample, $T_{\mathrm{m}}(r, I) \equiv T_{\mathrm{M}}(I) = T_{\mathrm{M}}$, where $I(A)$ is the intensity of the electrical dc. The crystallization process starts from $t = 0$, when an additional amount of energy per unit time is homogeneously released to the sample. The crystallization power density, W_{ef}, expressed in W m^{-3}, is

$$W_{\mathrm{ef}} = \Delta H_{\mathrm{eff}} \frac{\mathrm{d}x(t)}{\mathrm{d}t}, \tag{52}$$

where ΔH_{eff} is the amount of the total density of crystallization heat effectively contributing to the extra heating of the AGCM, and relative crystallinity (the volume fraction crystallized with time) $x(t)$ represents the solution of the JMA equation [22]. At the initial moment, $t = 0$, the transformed volume fraction is $x(0) = 0$, while at the equilibrium of the crystalline phase, $x(t \to \infty) = 1$.

During the sample's crystallization, the energetic balance between the crystallization power density (52), the heat developed in the unit volume of the metallic core by the joule effect,

$$W_i = \rho(t)\frac{I^2}{S^2}, \tag{53}$$

and the radiative heat loss simply reads

$$\rho_{\mathrm{M}} c \frac{\mathrm{d}T(t)}{\mathrm{d}t} = W_{\mathrm{ef}}(t) + \rho(t)\frac{I^2}{S^2} - P\left[T^4(t) - T_{\mathrm{M}}^4\right], \tag{54}$$

where

$$\rho(t) = \rho_{\mathrm{amorph}}(t)\left[1 - x(t)\right] + \rho_{\mathrm{crys}}(t)x(t) \tag{55}$$

is the electrical resistivity of the AGCM during the crystallization process. In this equation

$$\rho_{\mathrm{amorph}}(t) = \rho_{\mathrm{m}}\left\{1 + \alpha_{\mathrm{amorph}}\left[T(t) - T_{\mathrm{M}}\right]\right\} \tag{56}$$

represents the electrical resistivity of the amorphous phase, α_{amorph} is the corresponding thermal coefficient of this resistivity, while

$$\rho_{\mathrm{crys}}(t) = \rho_{\mathrm{m}}\left\{1 + \alpha_{\mathrm{crys}}\left[T(t) - T_{\mathrm{M}}\right]\right\} \tag{57}$$

represents the electrical resistivity of the crystalline phase, where α_{crys} is the corresponding thermal coefficient.

Thus, at the initial moment, $t = 0$, the electrical resistivity is $\rho(t = 0) = \rho_{\mathrm{amorph}}(t = 0) = \rho_{\mathrm{m}}$, i.e., the sample as a whole is in the amorphous state, while at the equilibrium of the crystalline phase the electrical resistivity is given by $\rho(t \to \infty) = \rho_{\mathrm{crys}}(t)$ (the sample is completely crystallized).

Introducing (55) and (56) in (57) one can obtain the electrical resistivity $\rho(t)$ of the AGCM during the crystallization process:

$$\rho(t) = \rho_{\mathrm{m}}\left\{1 + \alpha_{\mathrm{amorph}}\left[T(t) - T_{\mathrm{M}}\right]\right\} + \rho_{\mathrm{m}}(\alpha_{\mathrm{crys}} - \alpha_{\mathrm{amorph}})\left[T(t) - T_{\mathrm{M}}\right]x(t). \tag{58}$$

In the case of joule heating, an increase of electrical resistivity implies a corresponding increase of the joule power, and subsequently a rapid increase of the sample's temperature. The kinetics of this process must be studied in order to precisely control the structural transformations of the AGCM during the crystallization process. In the non-isothermal crystallization process of the sample, energetic balance between the crystallization power density (52), the heat developed in the unit volume by the joule effect in the metallic core (53) and radiative heat loss is given by

$$\rho_{\mathrm{M}} c \frac{\mathrm{d}T(t)}{\mathrm{d}t} = \Delta H_{\mathrm{eff}} n\left[1 - x(t)\right]\left\{-\ln\left[1 - x(t)\right]\right\}^{(n-1)/n} K_0^{1/n} \exp\left(-\frac{Q}{kT}\right)$$
$$- P\left[T^4(t) - T_{\mathrm{M}}^4\right] + \rho_{\mathrm{m}}\frac{I^2}{S^2} + \rho_{\mathrm{m}}\left[\gamma x(t) + \alpha_{\mathrm{amorph}}\right]\left[T(t) - T_{\mathrm{M}}\right]\frac{I^2}{S^2}, \tag{59}$$

where $\gamma = \alpha_{\mathrm{crys}} - \alpha_{\mathrm{amorph}}$.

The relations (51) and (59) form a differential equation system with the unknown quantities $T(t)$ and $x(t)$. Passing through the sample an electrical dc of $I(A) = 17.8$ mA, from (46) we obtain the equilibrium temperature of the amorphous phase at the initial moment, $T_{\mathrm{M}} = 248\,^{\circ}\mathrm{C}$. By best fit to experimental data we consider the same particular values for the adjustable parameters (the kinetic exponent $n = 3, 6$ and $\Delta H_{\mathrm{eff}} = 5.5 \times 10^8\ \mathrm{J\,m^{-3}}$). Also, in our numerical analysis we consider that in the non-isothermal crystallization process the growth or diffusion activation energy is $Q = 2.24$ eV.

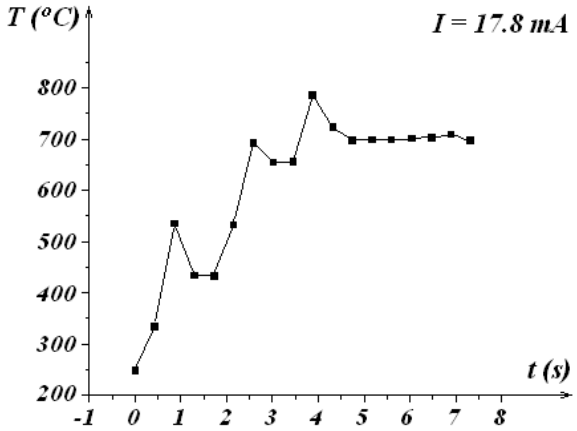

Figure 5. The temporal evolution of temperature, $T(t)$, in the non-isothermal crystallization process.

The numerical solution of the above mentioned differential equation system (i.e. the temperature $T(t)$ of the sample for an applied electrical dc of $I(A) = 17.8$ mA) is presented in figure 5. We observe that the entire non-isothermal crystallization process predicted by this model ranges from 248 to 800 °C. The numerical analysis gives for the AGCM's temperature three relative maximum values, corresponding to three successive stages of crystallization, as follows: the first stage corresponds to the temperature $T_{x_1} = 535\,^{\circ}\mathrm{C}$ and the second one to $T_{x_2} = 689\,^{\circ}\mathrm{C}$, while the third stage appears at $T_{x_3} = 784\,^{\circ}\mathrm{C}$. Structurally speaking, the first temperature corresponds to the formation of αFe(Si) phase, the second one to the precipitation of Fe_2B and the third one to $Fe_{23}B_6$.

This behaviour is in good agreement with the experimental results obtained by differential scanning calorimetry (DSC) and presented in figure 6. This figure shows the dependence of the heat flow as a function of temperature (in °C) for two different heating rates. As one can see, for a heating rate of 20 K min^{-1} the DSC curve exhibits two sharp peaks at $T_1 = 540\,^{\circ}\mathrm{C}$ and $T_2 = 685\,^{\circ}\mathrm{C}$ and also a third flattened peak centred on $T_3 = 780\,^{\circ}\mathrm{C}$.

3.2.2. Stress calculation during the crystallization process. The results regarding the spatio-temporal temperature distribution already obtained in section 3.1.1 and synthesized in figure 3 allow us to consider that, with a very good approximation, the temperature is constant in the section of the microwire. With this conclusion, the relations (1)–(4) (which constitute the basis of the model for the determination of the internal stresses induced in AGCM) become

$$\frac{\mathrm{d}}{\mathrm{d}r}\left[\frac{1}{r}\frac{\mathrm{d}(ru_r^{\mathrm{m}})}{\mathrm{d}r}\right] = 0, \tag{60a}$$

$$\frac{\mathrm{d}u_z^{\mathrm{m}}}{\mathrm{d}z} = \text{constant}, \tag{60b}$$

and

$$\frac{\mathrm{d}}{\mathrm{d}r}\left[\frac{1}{r}\frac{\mathrm{d}(ru_r^{\mathrm{g}})}{\mathrm{d}r}\right] = 0, \tag{61a}$$

$$\frac{\mathrm{d}u_z^{\mathrm{g}}}{\mathrm{d}z} = \text{constant}. \tag{61b}$$

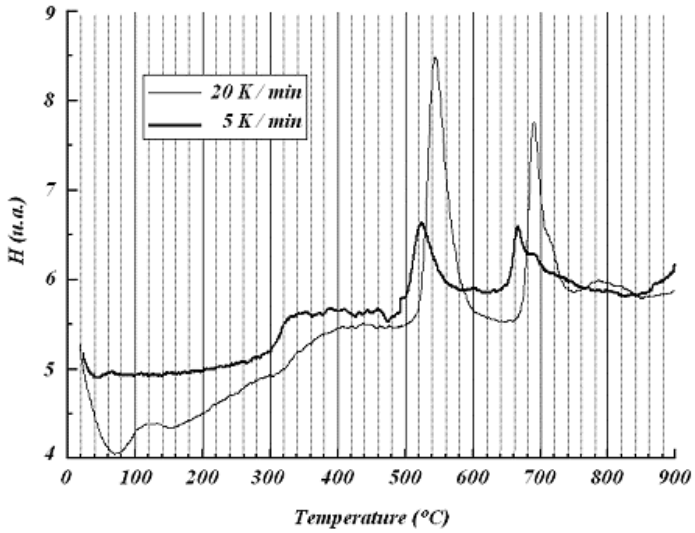

Figure 6. The DSC curves for $Fe_{77.5}Si_{7.5}B_{15}$ AGCMs.

The solutions of equations (60) are

$$u_r^{\mathrm{m}}(r) = C_1^{\mathrm{m}} r, \tag{62a}$$

and

$$u_z^{\mathrm{m}} = b_{\mathrm{m}} z, \tag{62b}$$

where we have taken into account that u_r^{m} $(r = 0)$ must be finite; this fact implies the cancellation of the term which contains the second integration constant. In the same manner, for equations (61) we can find the following solutions:

$$u_r^{\mathrm{g}}(r) = C_1^{\mathrm{g}} r + \frac{C_2^{\mathrm{g}}}{r} \tag{63a}$$

and

$$u_z^{\mathrm{g}} = b_{\mathrm{g}} z. \tag{63b}$$

In the above relations, C_1^{m}, b_{m}, C_1^{g}, C_2^{g} and b_{g} are integration constants.

Using the method already presented in section 2 and taking into account the constant value of the temperature in the section of the microwire (i.e. the null temperature gradients), for the stresses in the metallic core of the sample we obtained

$$\sigma_{rr}^{\mathrm{m}} = \frac{E_{\mathrm{m}}}{(1+\mu)(1-2\mu)} \left(C_1^{\mathrm{m}} + \mu b_{\mathrm{m}}\right), \tag{64a}$$

$$\sigma_{\theta\theta}^{\mathrm{m}} = \frac{E_{\mathrm{m}}}{(1+\mu)(1-2\mu)} \left(C_1^{\mathrm{m}} + \mu b_{\mathrm{m}}\right) \tag{64b}$$

and

$$\sigma_{zz}^{\mathrm{m}} = \frac{2E_{\mathrm{m}}\mu}{(1+\mu)(1-2\mu)}\left(C_1^{\mathrm{m}} + \mu b_{\mathrm{m}}\right) + E_{\mathrm{m}} b_{\mathrm{m}}, \tag{64c}$$

while for the glass cover we have found

$$\sigma_{rr}^{\mathrm{g}} = \frac{E_{\mathrm{g}}}{(1+\mu)(1-2\mu)}\left(C_1^{\mathrm{g}} + \mu b_{\mathrm{g}}\right) - \frac{E_{\mathrm{g}}}{1+\mu}\frac{C_2^{\mathrm{g}}}{r^2}, \tag{65a}$$

$$\sigma_{\theta\theta}^{\mathrm{g}} = \frac{E_{\mathrm{g}}}{(1+\mu)(1-2\mu)}\left(C_1^{\mathrm{g}} + \mu b_{\mathrm{g}}\right) + \frac{E_{\mathrm{g}}}{1+\mu}\frac{C_2^{\mathrm{g}}}{r^2} \tag{65b}$$

and

$$\sigma_{zz}^{\mathrm{g}} = \frac{2E_{\mathrm{g}}\mu}{(1+\mu)(1-2\mu)}\left(C_1^{\mathrm{g}} + \mu b_{\mathrm{g}}\right) + E_{\mathrm{g}} b_{\mathrm{g}}. \tag{65c}$$

The five integration constants can be determined with the aid of the same above mentioned five conditions (19)–(23), taking into account the different heating of the two materials with different thermal expansion coefficients. For this purpose we will use the expression which gives the resultant strain due to the heating of the two materials. Following [23] we suppose that the thermal expansion coefficient of the metallic core during the crystallization process is written as a function of volume fraction crystallized with time, $x(t)$, as follows:

$$\alpha_{\mathrm{m}} = \alpha_{\mathrm{amorph}}\left[1 - x(t)\right] + \alpha_{\mathrm{crys}} x(t). \tag{66}$$

Thus, at the initial instant of time, $t = 0$, the thermal expansion coefficient of the metal is $\alpha_{\mathrm{m}}(t = 0) = \alpha_{\mathrm{amorph}}$ (i.e., the sample as a whole is in the amorphous state), while at the equilibrium of the crystalline phase the thermal expansion coefficient is given by $\alpha(t \to \infty) = \alpha_{\mathrm{crys}}$ (the sample is completely crystallized). The resultant strain will be

$$\begin{aligned}\varepsilon = \varepsilon_{\mathrm{m}} - \varepsilon_{\mathrm{g}} = (\alpha_{\mathrm{m}} - \alpha_{\mathrm{g}})\left[T(t) - T_{\mathrm{M}}\right] = \left[(\alpha_{\mathrm{amorph}} - \alpha_{\mathrm{g}})\right. \\ \left. + (\alpha_{\mathrm{crys}} - \alpha_{\mathrm{amorph}})x(t)\right]\left[T(t) - T_{\mathrm{M}}\right].\end{aligned} \tag{67}$$

Using (62), (63), (64*a*), (64*c*), (65*a*), (65*c*) and (67) in (19)–(23) an algebraic system with five equations results, for the five unknown constants: C_1^{m}, b_{m}, C_1^{g}, C_2^{g} and b_{g}. Fortunately, this system can be solved analytically. The solution of this system (more precisely, only C_1^{m} and b_{m}) is needed for the determination of the expressions for the internal stresses induced in the AGCM's metallic core during the crystallization process. We get

$$\sigma_{rr}^{\mathrm{m}} = \sigma_{\theta\theta}^{\mathrm{m}} = \frac{3E_{\mathrm{g}}E_{\mathrm{m}}S[(\alpha_{\mathrm{amorph}} - \alpha_{\mathrm{g}}) + (\alpha_{\mathrm{crys}} - \alpha_{\mathrm{amorph}})x(t)](T(t) - T_{\mathrm{M}})}{(E_{\mathrm{g}} + 3E_{\mathrm{m}})S + 4E_{\mathrm{m}}} \tag{68a}$$

and

$$\sigma_{zz}^{\mathrm{m}} = \sigma_{rr}^{\mathrm{m}}\frac{(E_{\mathrm{g}} + E_{\mathrm{m}})S + 2E_{\mathrm{m}}}{E_{\mathrm{g}}S + E_{\mathrm{m}}}. \tag{68b}$$

As we expected, the internal stresses induced in this stage of the thermal treatment depend only on time. The dependences $\sigma_{rr}^{\mathrm{m}} = \sigma_{rr}^{\mathrm{m}}(t)$, $\sigma_{\theta\theta}^{\mathrm{m}}(= \sigma_{rr}^{\mathrm{m}}) = \sigma_{\theta\theta}^{\mathrm{m}}(t)$ and $\sigma_{zz}^{\mathrm{m}} = \sigma_{zz}^{\mathrm{m}}(t)$ are shown in figure 7. As this figure shows, there is no major difference between their temporal variation (the two curves have approximately the same shape) except the magnitude of the maximum values reached by the two stresses ($\sigma_{rr}^{\mathrm{m}} = \sigma_{\theta\theta}^{\mathrm{m}}$ and σ_{zz}^{m}).

Also, as one can see, the most significant temporal variation of the stresses induced in the crystallization process appears during the first crystallization stage, which corresponds to the formation of αFe(Si) phase. After the precipitation of this compound, the stresses tends rapidly to certain constant values which correspond to the equilibrium of the fully crystallized sample (about 271 MPa for $\sigma_{rr}^{\mathrm{m}} = \sigma_{\theta\theta}^{\mathrm{m}}$ and 761 MPa for σ_{zz}^{m}).

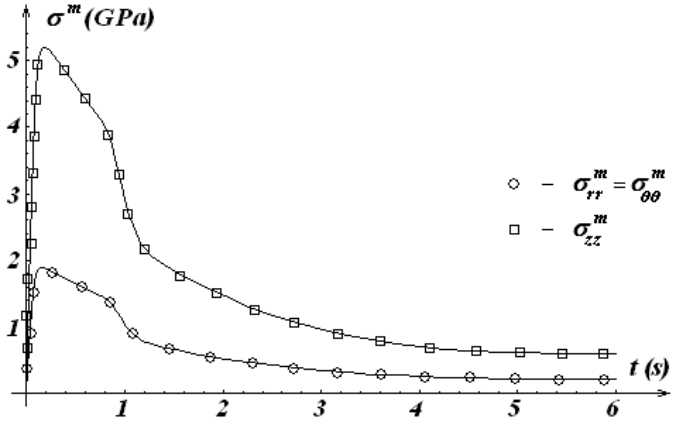

Figure 7. Temporal variation of the internal stresses induced in the AGCM during the crystallization process.

3.3. Internal stresses induced in the AGCM during the cooling from T_∞^{crys} to room temperature

3.3.1. Temperature distribution in the sample during the cooling process from T_∞^{crys} to room temperature

(a) In the metallic core. The next stage of the thermal treatment is the cooling of the sample from the equilibrium temperature of the crystalline phase, T_∞^{crys}, to room temperature, T_w. As already known, in order to determine the internal stresses induced in the AGCM during the cooling process, we must first get the temperature distribution in the sample. This temperature distribution results as the solution of the Fourier heat equation. Keeping in mind the spatial symmetry of the problem, we will write this equation in a cylindrical coordinate system:

$$\frac{\partial T_1}{\partial t} = a_1 \left(\frac{\partial^2 T_1}{\partial r^2} + \frac{1}{r} \frac{\partial T_1}{\partial r} \right). \tag{69}$$

The solution of this equation is

$$T_1(r,t) = T_w + (T_\infty^{\text{crys}} - T_w) \sum_{j=1}^{\infty} \frac{2J_0(\beta_j \frac{r}{R})}{\beta_j J_1(\beta_j)} \exp\left(-\frac{a_1 \beta_j^2}{R^2} t \right), \tag{70}$$

where $J_0(\beta_j \frac{r}{R})$ and $J_1(\beta_j)$ are the zeroth and first order Bessel functions respectively, β_j are the solutions of the characteristic equation $J_0(\beta) = 0$ and $a_1 = \frac{k_{\text{m}}}{\rho_{\text{m}} c_p}$. We also used the boundary conditions $T_1(r,0) = T_\infty^{\text{crys}}$ and $(-\frac{\partial T}{\partial r})_{r=R} = 0$. The expression (70) represents the spatio-temporal distribution of the temperature in the sample during the cooling process. Separately, these two dependences (radial and temporal) appear as in figures 8 and 9 respectively.

Figure 8 shows the spatial (radial) distribution of the temperature in the metallic core of the AGCM after $t = 0.2$ μs from the beginning of the cooling process, while figure 9 shows the temporal evolution of the temperature in the centre of the AGCM. Both dependences were drawn for the same sample, having $R_{\text{m}} = 3.65$ μm and $R_{\text{w}} = 11.30$ μm. From figure 8 we observe that the difference between the temperature in the centre of the AGCM and at the point $r = R_{\text{m}}$ is very small (being about 7.469×10^{-9} °C). Consequently, we may consider that the sample cools uniformly in its cross-section during the cooling process. Besides, this feature

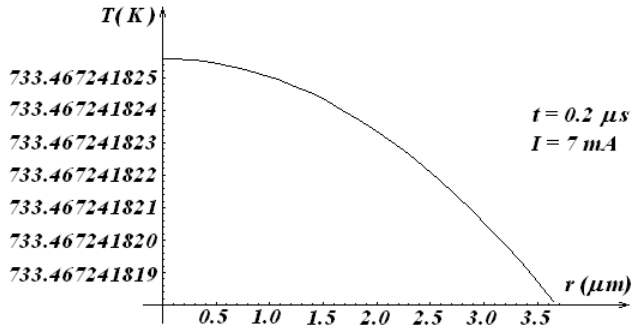

Figure 8. Radial temperature distribution after $t = 0.2\ \mu$s from the beginning of the cooling process.

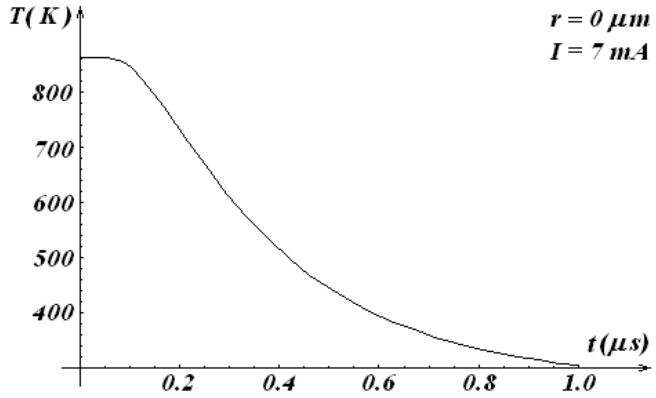

Figure 9. Temporal distribution of the temperature in the metallic core during the cooling process.

persists during the whole cooling process. As for the time needed for the sample to reach room temperature, as figure 9 shows, it is of the order of micro-seconds.

(b) In the glass cover. Except the boundary conditions and the constant a_1 (here $a_1 \to a_2 = \frac{k_g}{\rho_g c_g}$), this problem coincides with that given in the previous paragraph. So, the Fourier heat equation will be

$$\frac{\partial T_2}{\partial t} = a_2 \left(\frac{\partial^2 T_2}{\partial r^2} + \frac{1}{r} \frac{\partial T_2}{\partial r} \right), \qquad R_m < r < R_w, \tag{71}$$

with the following boundary conditions:

$$T_2(r, 0) = T_\infty^{crys}, \qquad T_1(r = R_m, t) = T_2(r = R_m, t), \qquad T_2(r = R_m, t = 0) = T_\infty^{crys},$$
$$T_2(r = R_w, t = 0) = T_w.$$

Its solution is given by

$$T_2(r, t) = \pi (T_\infty^{crys} - T_w) \sum_{j=1}^{\infty} \frac{J_0^2(\alpha_j) Z_0(\alpha_j r / R_m) \exp[-a_1 \alpha_j^2 t / R_m^2]}{J_0^2(\alpha_j) - J_0^2(\alpha_j R_w / R_m)}$$
$$+ \frac{T_\infty^{crys} \ln\left[R_w / r\right] + T_w \ln\left[r / R_m\right]}{\ln\left[R_w / R_m\right]}, \tag{72}$$

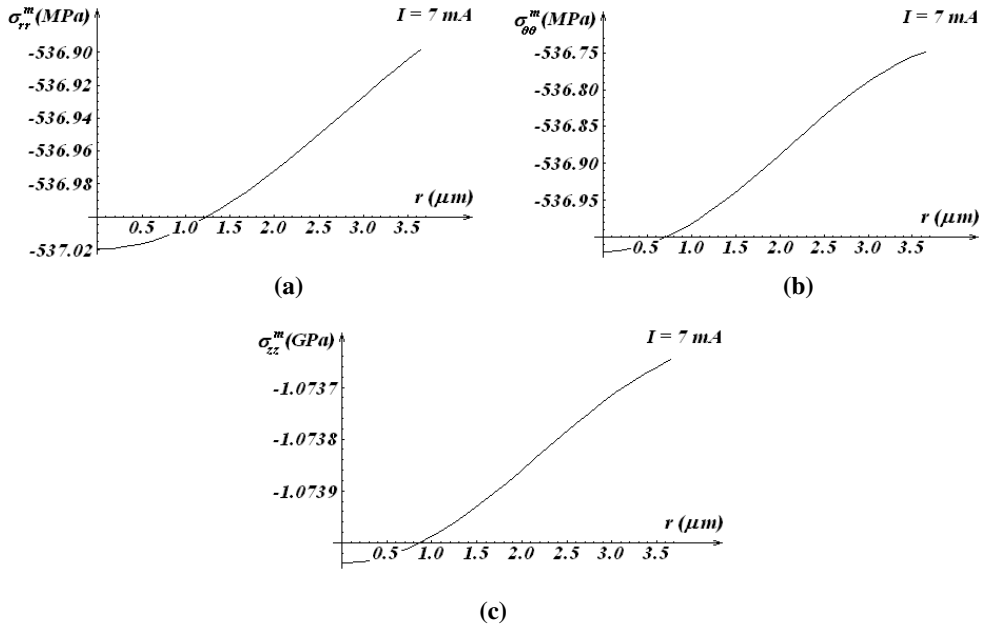

Figure 10. Internal radial, azimuthal and axial stresses induced during the cooling process.

where

$$Z_0(\alpha_j r/R_{\rm m}) = N_0(\alpha_j R_{\rm w}/R_{\rm m})J_0(\alpha_j r/R_{\rm m}) - N_0(\alpha_j r/R_{\rm m})J_0(\alpha_j R_{\rm w}/R_{\rm m}). \tag{73}$$

In the above relation $J_0(\alpha_j r/R_{\rm m})$ are the first order Bessel functions, $N_0(\alpha_j r/R_{\rm m})$ are the Neumann functions, $a_2 = \frac{k_{\rm g}}{\rho_{\rm g} c_{\rm g}}$, and α_j are the roots of the characteristic equation:

$$\frac{J_0(\alpha)}{J_0(\alpha R_{\rm w}/R_{\rm m})} = \frac{N_0(\alpha)}{N_0(\alpha R_{\rm w}/R_{\rm m})}. \tag{74}$$

3.3.2. Internal stresses induced in the AGCM during the cooling process. In order to find the internal stresses induced in the AGCM during the cooling process we use (70) and (72) in (13) and (14) (where one has to notice that T_2 in relation (72) represents in fact $t(r)$ from relations (14)), then to find the integration constants $C_1^{\rm m}$, $C_1^{\rm g}$, $C_2^{\rm g}$, $b_{\rm m}$ and $b_{\rm g}$ we must assume the condition set (19)–(23). The final form for $\sigma_{rr}^{\rm m}$, $\sigma_{\theta\theta}^{\rm m}$ and $\sigma_{zz}^{\rm m}$ result by substituting the already obtained constants in (13) and (14).

We preferred to give a graphic solution. The three stresses $\sigma_{rr}^{\rm m}$, $\sigma_{\theta\theta}^{\rm m}$ and $\sigma_{zz}^{\rm m}$ were represented in figure 10.

As one can see, all three stresses exhibit the same behaviour for this phase of the thermal treatment. The three curves show a continuous increasing of the stresses, which are compressive everywhere in the range $(0, R_{\rm m})$.

Briefly, in this section we calculated the thermal stresses that correspond to the successive heating, crystallization and cooling treatments of the AGCM, taking into account the differences between the thermal expansion coefficients of metal and glass.

Therefore, during the heating of the amorphous state, when the temperature values are below the onset temperature of crystallization we have found that

- for higher value of the applied dc current the maximum value of the temperature is reached faster,

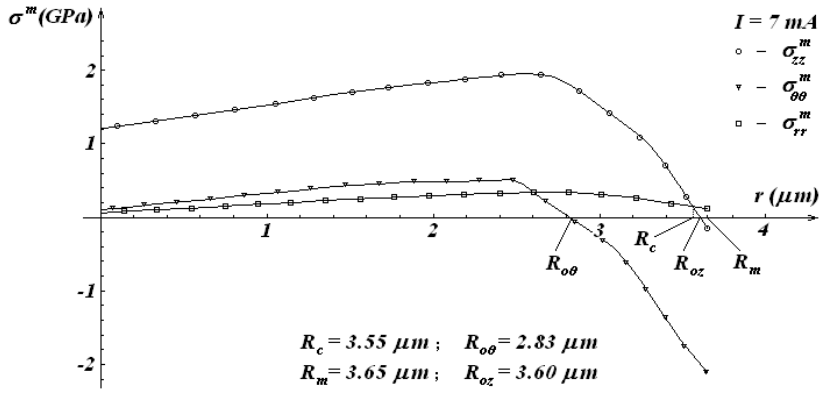

Figure 11. The internal total stresses induced in the AGCM during the thermal treatment (heating–crystallization–cooling) and considering the supplementary stresses induced by the continuous drawing.

- for a specified value of the dc current the temperature is practically constant in the metallic core's cross section,
- in the AGCM's cross section the internal stresses present a continuous increasing of their values from the AGCM's centre to the metal–glass interface, where they reach the maximum values, close to 10^8 Pa,
- for a specified radius of the metallic core, the values of the stresses in the metallic core increase with the glass cover thickness, so a higher value of the stresses corresponds to a higher value of the glass cover thickness;
- for a specified value of the glass cover's thickness, a smaller value of the stresses in the metallic core corresponds to a higher metallic core radius;
- smaller internal stresses are obtained at higher values of the electric dc current.

Also, during the crystallization process, the AGCM's temperature has three relative maximum values, that correspond to the three successive stages of crystallization. The first maximum of the temperature corresponds to the formation of the αFe(Si) phase, the second one to the precipitation of the Fe_2B and the third one to the formation of the $Fe_{23}B_6$. During the first crystallization stage, the induced stresses present a significant temporal variation (see figure 7). After the precipitation of αFe(Si) phase, the stresses tend rapidly to certain constant values which correspond to the equilibrium of the fully crystallized sample.

In the last stage of the thermal treatment, during the cooling of the AGCM, the compressive stresses are in the range $(0, R_{\mathrm{m}})$.

4. Results and discussion

All the considerations below refer to the same AGCM as studied above, having $R_{\mathrm{m}} = 3.65\ \mu$m and $R_{\mathrm{w}} = 11.30\ \mu$m. The total stresses are calculated by adding to the internal stresses induced in the preparation process (found in [4]) the different stress components induced in the three considered stages of the thermal treatment (heating–crystallization–cooling). The total stress distribution is illustrated in figure 11. We mention that, in order to draw the curves for $\sigma^{\mathrm{m}}_{rr}(r)$, $\sigma^{\mathrm{m}}_{\theta\theta}(r)$ and $\sigma^{\mathrm{m}}_{zz}(r)$, we have also considered the supplementary 'frozen-in' internal stresses induced in the preparation process of the AGCM due to its continuous mechanical drawing [4]. It is very difficult to calculate the exact magnitude and distribution of these stresses, since

the microwire is not for its entire length in the elastic strains' domain. We have determined these stresses in an indirect way, by taking into account the distribution of the added stresses and the results of magnetic measurements in the framework of the analogy with the case of conventional microwires.

From figure 11 one can observe that the shape of the $\sigma^{\mathrm{m}}_{\theta\theta}(r)$ and $\sigma^{\mathrm{m}}_{zz}(r)$ curves is the same, but the positive values of $\sigma^{\mathrm{m}}_{zz}(r)$ are almost four times the positive values of $\sigma^{\mathrm{m}}_{\theta\theta}(r)$. The $\sigma^{\mathrm{m}}_{\theta\theta}(r)$ curve shows a positive maximum value of about $\sigma^{\mathrm{m}}_{\theta\theta}(r) \approx 500$ MPa at $r \cong 2.48$ μm, and $\sigma^{\mathrm{m}}_{zz}(r)$ curve shows its positive maximum value of about $\sigma^{\mathrm{m}}_{zz}(r) \approx 1950$ MPa at $r \cong 2.6$ μm. After reaching the maximum, both $\sigma^{\mathrm{m}}_{zz}(r)$ and $\sigma^{\mathrm{m}}_{\theta\theta}(r)$ decrease, reaching near the surface of the metal a small negative value (about -180 MPa for $\sigma^{\mathrm{m}}_{zz}(3.65\ \mu\mathrm{m})$) and a respectively high negative value (about -2100 MPa for $\sigma^{\mathrm{m}}_{\theta\theta}(3.65\ \mu\mathrm{m})$). $\sigma^{\mathrm{m}}_{rr}(r)$ has a much moderate variation than $\sigma^{\mathrm{m}}_{zz}(r)$ and $\sigma^{\mathrm{m}}_{\theta\theta}(r)$, having only positive values. Thus, the radial stresses are tensile everywhere in the range $(0, R_{\mathrm{m}})$, while the azimuthal and axial ones are tensile from $r = 0$ to approximately $R_{o\theta} \cong 2.83$ μm (77.53% of R_{m}) for $\sigma^{\mathrm{m}}_{\theta\theta}(r)$ and respectively, $R_{oz} = 3.60$ μm (98.63% of R_{m}) for $\sigma^{\mathrm{m}}_{zz}(r)$, changing sign close to the surface, where they become compressive. The $\sigma^{\mathrm{m}}_{rr}(r)$ curve reaches a maximum value at $r \cong 2.86$ μm of $\cong$300 MPa, then it decreases with a slope of an absolute value higher than that of the ascendant portion of the curve (until it reaches the maximum value). As one can see, $\sigma^{\mathrm{m}}_{zz}(r)$ and $\sigma^{\mathrm{m}}_{\theta\theta}(r)$ do not intersect each other, both being intersected by $\sigma^{\mathrm{m}}_{rr}(r)$. The intersection point between $\sigma^{\mathrm{m}}_{zz}(r)$ and $\sigma^{\mathrm{m}}_{rr}(r)$ is at $R_c \cong 3.55$ μm (approximately 97.26% of R_{m}).

Starting from the point $r = 0$ up to the point $R_c \cong 3.55$ μm there is a region in which $\sigma^{\mathrm{m}}_{zz}(r)$ is the component with the highest value and it is positive (zone I). From this point to the point $R_{oz} = 3.60$ μm there is a second region, much narrower than the first one, in which $\sigma^{\mathrm{m}}_{rr}(r)$ is the highest stress component and it is also positive (zone II). The remaining part of the microwire (up to the metal–glass interface) constitutes a third region, dominated by the negative values (compression) of $\sigma^{\mathrm{m}}_{zz}(r)$ and $\sigma^{\mathrm{m}}_{\theta\theta}(r)$ (zone III).

As is well known, the alloy to which we have referred is highly magnetostrictive. This feature leads to a strong coupling between the internal stresses and the magnetostriction. This coupling determines the appearance in the metallic part of the AGCM of the easy axes of magnetization in the directions in which the dominant internal stresses are tensile (positive), and respectively of the hard axes of magnetization in the directions in which the dominant stresses are compressive (negative). So, the magnetoelastic energy minimization leads to a domain structure which presents three zones:

- zone I, $r \in [0, R_c)$; due to the coupling between $\sigma^{\mathrm{m}}_{zz}(r)$ (positive) and the magnetostriction the first zone results, with an uniaxial magnetic anisotropy having the easy axis oriented along the axis of the AGCM (Oz-axis);
- zone II, $r \in (R_c, R_{0z})$; due to the coupling between $\sigma^{\mathrm{m}}_{rr}(r)$ (positive) and the magnetostriction the second zone results, with a radial magnetic anisotropy (also, in this zone the compressive component $\sigma^{\mathrm{m}}_{\theta\theta}(r)$ generates a hard axis of magnetization in the azimuthal direction);
- zone III, $r \in (R_{0z}, R_{\mathrm{m}}]$; in this zone the two compressive components ($\sigma^{\mathrm{m}}_{\theta\theta}(r)$ and $\sigma^{\mathrm{m}}_{zz}(r)$) generate two hard axes of magnetization in the azimuthal direction and in the axial direction respectively. Also, this zone presents a third (easy) axis of magnetization which appears because of the coupling between the $\sigma^{\mathrm{m}}_{rr}(r)$ (positive) and the magnetostriction.

Synthesizing, we can state that the stress distribution from figure 11, coupled with the high positive magnetostriction of the $Fe_{77.5}Si_{7.5}B_{15}$ alloy, leads in a first order approximation to an easy axis distribution associated with a domain structure which consists of a cylindrical inner

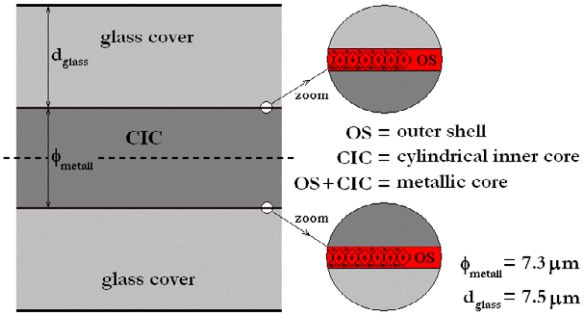

Figure 12. Schematic diagram of the estimated domain structure in positive magnetostrictive AGCMs.

core (CIC) with axial magnetization (zone I) and an outer shell (OS) with radial magnetization (zone II plus zone III) (see figure 12).

The above mentioned domain structure depends on the distribution of the total internal stresses that appear both in the preparation process of the AGCM and in the whole thermal treatment (heating–crystallization–cooling) and which, in turn, strongly depends on the diameter of the metallic part of the AGCM and on the thickness of the glass cover.

Let us now analyse the changes that appear in the magnetic domain structure of the microwire's metallic part due to the thermal treatment, in comparison with that obtained from the preparation process. From this analysis we may find the influence of the thermal treatment on the AGCM's magnetic properties.

From figure 11 one can observe that the maximum value of the axial stresses obtained after the thermal treatment is bigger than that obtained in the preparation process (for comparison see the figure 6 in [4]); this difference is about 450 MPa. On the other hand, the maximum values for the azimuthal and radial stresses decrease by $\cong$220 MPa and respectively $\cong$210 MPa.

But most important, the intersection point between $\sigma_{zz}^{m}(r)$ and $\sigma_{rr}^{m}(r)$ (which before the thermal treatment is at 84.6% of R_m) moved away to 97.26% of R_m. This means that zone I enlarged significantly, by $\cong$13%. Obviously, this difference must be found again in the smaller dimensions of the remaining zones II and III. Indeed, both zone II and zone III became narrower by $\cong$2% and respectively $\cong$11%. In other words, the cylindrical inner core with radius R_c which forms the first magnetic domain with uniaxial magnetic anisotropy grows up by about 13%, while the other two magnetic domains delimited by the zone II and zone III decrease by about the same value (13%—together). This involves the increase of the degree of magnetic order in the sample. The first observation we made here acts in the same direction. More explicitly, the increase of the maximum value of the internal axial stresses against the radial and azimuthal ones produces a stronger magnetic coupling between the magnetostriction and $\sigma_{zz}^{m}(r)$. These two features lead to the appearance of a large Barkhausen effect (LBE) in low axially applied magnetic fields. Such a domain structure favours the appearance of the LBE; the previous studies have demonstrated that the axial inner core is the effective region in which nucleation and propagation take place, i.e., this zone is responsible for the appearance of the LBE [24]. Following [25], the increase of the cylindrical inner core's dimensions leads to a corresponding increase of the remanent magnetization M_r:

$$M_r = M_s \left(\frac{R_c}{R_m} \right)^2, \tag{75}$$

where M_s is the saturation magnetization. Thus, the theoretical evaluations referring only to

the preparation process of the AGCM, without considering the supplementary axial tensile stresses induced in the preparation process due to its continuous mechanical drawing, give for the ratio $\frac{M_r}{M_s}$ a value of about 0.72 [4], which differs by the measured value that would correspond (through relation (75)) to a radius of the cylindrical inner core of about 94.8% of R_{m}. If these supplementary axial tensile stresses are considered, the value of the ratio $\frac{M_r}{M_s}$ grows up to 0.9, which is close to the correct (experimental) value obtained by magnetic measurements performed using a fluxmeter method [26]; these magnetic measurements were performed at a maximum value of the axially applied field of 150 Oe, at a frequency of 400 Hz. The studied microwire ($R_{\mathrm{m}} = 3.65\ \mu$m, $d_{\mathrm{g}} = 7.5\ \mu$m) presents a bistable flux reversal phenomenon in low axial fields at 30 Oe. We mention that M_r is about 0.9 of M_s (measured at the maximum field). The value of M_s measured by the fluxmeter method is close to the value measured with the VSM (vibrating sample magnetometer) in a 1 T magnetic field. From the ratio $\frac{M_r}{M_s}$ (also called the reduced remanence) determined experimentally it follows that the radius of the cylindrical inner core is about $\cong$95% of R_{m}; i.e., it is very close to the determined value from theoretical considerations on the preparation process, also taking into account the supplementary axial tensile stresses due to continuous drawing of the microwire.

Our theoretical model on thermal treatment of the microwires considers the supplementary stresses due to the mechanical drawing of the microwire during the preparation process and gives for the ratio $\frac{M_r}{M_s}$ a value of about 0.95, which is in very good agreement with the experiment. Thus, we conclude that a proper thermal treatment (which must contain a fully crystallization stage) of an AGCM can be considered as a useful method for increasing the remanent magnetization M_r of an amorphous material.

Finally, we notice that the numerical values for the supplementary radial, circumferential (azimuthal) and axial stresses were determined by best fit to experimental data obtained by measuring the reduced remanence of the prepared microwires, after removal of the glass cover from the metallic core (using a chemical etching technique) and applying a suitable external axial tensile stress; the magnitude of this axial stress has been chosen such that the theoretical intersection point between the curve representing the radial distribution of the axial stresses $\sigma_{zz}^{\mathrm{m}}(r)$, and the curve that gives the radial distribution of the radial stresses $\sigma_{rr}^{\mathrm{m}}(r)$, overlaps at the intersection point corresponding to the experimental results. On the other hand, this supplementary axial stress produces in the other two directions (radial and azimuthal) corresponding transverse Poisson contractions (thus, the stresses in these directions are compressive). Supposing that the strains are elastic and homogeneous, we have

$$\sigma_{rr}^{\mathrm{suppl}} = \sigma_{\theta\theta}^{\mathrm{suppl}} = -\mu\sigma_{zz}^{\mathrm{suppl}}, \tag{76}$$

where $\sigma_{rr}^{\mathrm{suppl}}$, $\sigma_{\theta\theta}^{\mathrm{suppl}}$ and $\sigma_{zz}^{\mathrm{suppl}}$ are the radial, circumferential and axial stresses induced due to the mechanical drawing and μ is Poisson's coefficient. Using the spline method in order to model the dependences $\sigma_{rr}^{\mathrm{m}}(r)$ and $\sigma_{zz}^{\mathrm{m}}(r)$ as the polynomial functions $F_{rr}(r)$ and $F_{zz}(r)$, for the theoretical intersection point, $r = R_c^{\mathrm{theor}}$, we must have $F_{rr}(R_c^{\mathrm{theor}}) = F_{zz}(R_c^{\mathrm{theor}})$. But, taking into account the supplementary stress components, the intersection point becomes $r = R_c^{\mathrm{exper}}$ instead of $r = R_c^{\mathrm{theor}}$. So, assuming that the supplementary stresses do not depend on r, we must also have

$$F_{rr}\left(R_c^{\mathrm{exper}}\right) + \sigma_{rr}^{\mathrm{suppl}} = F_{zz}\left(R_c^{\mathrm{exper}}\right) + \sigma_{zz}^{\mathrm{suppl}}. \tag{77}$$

By solving the system of equations (76) and (77) for the considered microwire, we have obtained the desired values of these supplementary stresses.

5. Conclusions

In this paper we determined the values of the internal stresses induced in the radial, azimuthal and axial directions during the thermal treatment of the magnetic AGCM $Fe_{77.5}B_{15}Si_{7.5}$. These stresses are owing to the successive heating, crystallization and cooling of the metal as well as to contractions generated by the glass cover in the metal during the thermal treatment due to difference between the thermal expansion coefficients of metal and glass. The resultant stresses have values of an order of 10^9 Pa, that depend on the dimensions of the metallic part of AGCM and the glass cover.

Taking into account the high positive magnetostriction of the $Fe_{77.5}B_{15}Si_{7.5}$ alloy, the following magnetic domain structure results: between $r = 0$ and $r = R_c$ a zone with a uniaxial magnetic anisotropy appears, having the easy axis oriented along the axis of the AGCM (Oz-axis) due to the coupling between $\sigma_{zz}^{\mathrm{m}}(r)$ (positive) and the magnetostriction; between $r = R_c$ and $r = R_{0z}$ a zone with a radial magnetic anisotropy appears, due to the coupling between $\sigma_{rr}^{\mathrm{m}}(r)$ (positive) and the magnetostriction. Also, in this zone the compressive component $\sigma_{\theta\theta}^{\mathrm{m}}(r)$ generates a hard axis of magnetization in the azimuthal direction; finally, between $r = R_{0z}$ and $r = R_{\mathrm{m}}$ we have a zone with two hard axes of magnetization (in the azimuthal direction and in the axial direction) generated by the two compressive components ($\sigma_{\theta\theta}^{\mathrm{m}}(r)$ and $\sigma_{zz}^{\mathrm{m}}(r)$ respectively). Also, this zone shows a third (easy) axis of magnetization, which appears because of the coupling between the $\sigma_{rr}^{\mathrm{m}}(r)$ (positive) and magnetostriction.

The changes appearing in the magnetic domain structure of the microwire's metallic part due to the thermal treatment, in comparison with that obtained from the preparation process, can be summarized in the following observations.

- The maximum value of the axial stresses obtained after the thermal treatment is higher than that obtained in the preparation process; this difference is about 450 MPa.
- The maximum values for the azimuthal and radial stresses decrease by $\widetilde{=}$220 MPa and respectively, $\widetilde{=}$210 MPa.
- The intersection point between $\sigma_{zz}^{\mathrm{m}}(r)$ and $\sigma_{rr}^{\mathrm{m}}(r)$ (which before the thermal treatment and without considering the supplementary stresses induced by the continuous drawing is at 84.6% of R_{m}) moved away to 97.26% of R_{m}. This means that zone I enlarged significantly (by $\widetilde{=}$13%), which involves the increase of the degree of magnetic order in the AGCM. Also, the increase of the maximum value of the internal axial stresses against the radial and azimuthal ones produces a stronger magnetic coupling between the magnetostriction and $\sigma_{zz}^{\mathrm{m}}(r)$. This feature led to the appearance of a large Barkhausen effect (LBE) in low axially applied magnetic fields.
- After the thermal treatment and consideration of supplementary stresses induced by the continuous drawing during the preparation process, the intersection point between $\sigma_{rr}^{\mathrm{m}}(r)$ and $\sigma_{zz}^{\mathrm{m}}(r)$ moved away from $\widetilde{=}$94.8% of R_{m} to 97.26% of R_{m}, which means that the reduced remanence increased from 0.90 to 0.95. The higher obtained values of the reduced remanence in highly magnetostrictive AGCM opens up a larger field of sensing applications for these microwires.

It is known that AGCMs are used for GMI measurements. Using these measurements information about evolution of magnetic structure with annealing can be obtained indirectly. P Tiberto *et al* [27] show that dc joule heating modifies the domain structures, enhancing the GMI response.

The theoretical model presented in this paper directly allows us to analyse the magnetic domains by the calculation of induced thermal stresses that appear in AGCM during both the preparation process and dc joule-heating thermal treatment (heating–crystallization–cooling).

Acknowledgment

The authors wish to thank Romanian CEEX POSTDOC-NANOSCIENCE for the financial support of this research.

References

[1] Chiriac H, Óvári T A, Vazquez M and Hernando A 1998 *J. Magn. Magn. Mater.* **205/206** 177
[2] Kraus L, Knobel M, Kane S N and Chiriac H 1999 *J. Appl. Phys.* **85** 5435–7
[3] Hagiwara M and Inoue A 1993 *Production Techniques of Alloy Wires by Rapid Solidification in Rapidly Solidified Alloys* ed H H Liebermann (New York: Dekker) p 141
[4] Chiriac H, Óvári T A and Pop Gh 1995 *Phys. Rev.* B **52** 10104
[5] Vázquez M, Gómez-Polo C, Chen D X and Hernando A 1994 *IEEE Trans. Magn.* **30** 907
[6] Chiriac H, Hristoforou E, Neagu M and Darie I 2001 *Mater. Sci. Eng.* A **304–306** 1011
[7] Chiriac H 1997 *Proc. Int. Conf. (Bangalore, 1997)*
[8] Chiriac H and Óvári T A 1996 Amorphous glass-covered magnetic wires: preparation, properties, applications *Prog. Mater. Sci.* **40** 333
[9] Allia P, Baricco M, Tiberto P and Vinai F 1993 *Rev. Sci. Instrum.* **64** 1053
[10] Allia P, Baricco M, Knobel M, Tiberto P and Vinai F 1994 *Mater. Sci. Eng.* A **179/180** 361
[11] Chiriac H, Knobel M and Óvári T A 1999 *Mater. Sci. Forum* **302** 239–43
[12] Chiriac H and Óvári T A 1998 *Non-Linear Electromagnetic Systems* (Amsterdam: IOS Press) p 243
[13] Chiriac H and Aştefănoaei I 1996 *Phys. Status Solidi* a **153** 183
[14] Lekhnitskii S G 1981 *Theory of Elasticity of an Anisotropic Body* (Moscow: Mir) p 19
[15] Bosley B A and Weiner J H 1960 *Theory of Thermal Stresses* (New York: Wiley) p 291
[16] Aştefănoaei I, Radu D and Chiriac H 2005 *J. Phys. D: Appl. Phys.* **38** 235
[17] Allia P, Baricco M, Knobel M, Tiberto P and Vinai F 1994 *Mater. Sci. Eng.* A **179/180** 361
[18] Zhang H and Mitchell B S 2000 *J. Mater. Res.* **15** 1000
[19] Schneider P J 1955 *Conduction Heat Transfer* (Reading, MA: Addison-Wesley)
[20] Kraus L, Chiriac H and Óvári T A 2000 *J. Magn. Magn. Mater.* **215/216** 343
[21] Christian J W 1975 *The Theory of Transformations in Metals and Alloys* (Oxford: Pergamon)
[22] Cahn R W (ed) 1970 *Physical Metallurgy* (Amsterdam: North-Holland) p 516
[23] Boyadjiev I, Thomson P F and Lam Y C 1996 *ISIJ Int.* **36** 1413
[24] Vázquez M and Chen D X 1995 *IEEE Trans. Magn.* **31** 1229
[25] Severino A M, Gomez-Polo C, Marin P and Vázquez M 1992 *J. Magn. Magn. Mater.* **103** 117
[26] Mandal K and Ghatak S K 1993 *J. Magn. Magn. Mater.* **118** 315
[27] Tiberto P, Coisson M, Vinai V and Kane S N 2002 *IEEE Trans. Magn.* **38** (5)